Transport Pathways of Peroxyacetyl Nitrate in the Upper Troposphere and Lower Stratosphere from different monsoon systems during the Summer Monsoon Season

Suvarna Fadnavis[1], Kirill Semeniuk[2], Martin G. Schultz[3] and Anoop Mahajan[1], Luca Pozzoli[4], Michael Kiefer[5], S. Sonbawane[1],
[1]Indian Institute of Tropical Meteorology, Pune India
[2]Department of Earth and Space Sciences and Engineering, York University, Toronto, Canada
[3]Institute for Energy and Climate Research-Troposphere (IEK-8), Forschungszentrum Jülich, Jülich, Germany
[4]Eurasia Institute of Earth Sciences, Istanbul Technical University, Turkey
[5]Karlsruhe Institute of Technology, Institute for Meteorology and Climate Research, Karlsruhe, Germany

Abstract:

The Asian summer monsoon involves complex transport patterns with large scale redistribution of trace gases in the upper troposphere and lower stratosphere (UTLS). We employ the global chemistry-climate model ECHAM5-HAMMOZ in order to evaluate the transport pathways and the contributions of nitrogen oxide species PAN, NO_x, and HNO_3 from various monsoon regions, to the UTLS over Southern Asia and vice versa. Simulated long term seasonal mean mixing ratios are compared with trace gas retrievals from the Michelson Interferometer for Passive Atmospheric Sounding (MIPAS-E) and aircraft campaigns during the monsoon season (June-September), since in these means typical patterns are expected to be the same.

The model simulations show that there are three regions which contribute substantial pollution to the UTLS during the monsoon: the Asian summer monsoon (ASM), the North American Monsoon (NAM) and the West African monsoon (WAM). However, penetration due to ASM convection is deeper into the UTLS as compared to NAM and WAM outflow. The circulation in these monsoon regions distributes PAN into the tropical latitude belt in the upper troposphere. Remote transport also occurs in the extratropical upper troposphere where westerly

winds drive North American and European pollutants eastward to partly merge with the ASM plume. Strong ASM convection transports these remote and regional pollutants into the lower stratosphere. In the lower stratosphere the injected pollutants are transported westward by easterly winds.

The intense convective activity in the monsoon regions is associated with lightning generation and thereby the emission of NOx. This will affect the distribution of PAN in the UTLS. The estimates of lightning produced PAN, HNO_3, NO_X and ozone obtained from control and lightning-off simulations shows high percentage changes over the regions of convective transport especially equatorial Africa and America and comparatively less over the ASM. This indicates that PAN in the UTLS over the ASM region is primarily of anthropogenic origin.

Introduction

Deep monsoon convection plays a key role in venting chemical constituents from the boundary layer and their export from source regions (Dickerson et al., 1987). The largest regional monsoon systems are the North American monsoon (NAM), Asian Summer Monsoon (ASM), Western North Pacific monsoon (WNPM), South American monsoon (SAM), West African Monsoon (WAM), and the Australian Monsoon (AUSM) (Chang et al., 2011). Recent observation and modeling studies indicate that the Asian summer monsoon (Park et al., 2004; Li et al., 2005; Randel and Park, 2006; Fu et al., 2006; Park et al., 2007; Xiong et al., 2009; Randel et al., 2010; Fadnavis et al., 2013), the North American Monsoon (Schmitz and Mullen 1996; Collier and Zhang, 2006; Barth et al., 2012) and the West African monsoon (Bouarar et al., 2011) play important roles in the transport of chemical constituents out of the boundary layer into the monsoon anticyclone in the upper troposphere and lower stratosphere. However, until now there has been no attempt to assess the relative contributions from these source regions and to analyze the transport patterns including possible recirculation within one consistent model framework. Model simulations also suggest that transported pollutants from the Asian monsoon region could contribute substantially to the budgets of stratospheric ozone, NO_X and water vapour (Randel et al., 2010). Transport of ozone precursors rich with VOCs during North American monsoon enhances ozone in the anticyclone (Li et al., 2005; Zhang et al., 2008; Choi et al., 2009; Barth et al., 2012). The deep monsoon convection over West Africa transports Central African emissions to the UTLS leading to large ozone changes in the lower stratosphere (Bouarar et al., 2011). A number of papers have reported transport of chemical constituents into the UTLS due to the Asian monsoon convection, less attention has been paid to deep convective

transport from North/South America and West Africa to the lower stratosphere and to their relative contributions to the UTLS composition over the ASM region.

Peroxyacetyl nitrate (PAN) is formed through oxidation of non methane volatile organic compounds (NMVOCs) in the presence of NO_X (Fischer et al., 2013). As discussed in Fischer et al. (2014), PAN is primarily formed after oxidation of acetaldehyde (CH_3CHO) and photolysis of acetone (CH_3COCH_3) and methyl glyoxal (CH_3COCHO), all of which are oxidation products of various NMVOCs. Globally, biogenic VOC like isoprene and terpenes contribute most, but in the context of our study it is important to note that the oxidation of most alkanes and alkenes which are often emitted from anthropogenic sources may also lead to PAN formation. PAN is formed in the reaction of the peroxy acetyl radical (CH_3CO_3) and NO_2. This reaction is reversible and the thermal decomposition of PAN back to CH_3CO_3 and NO_2 is the main sink of PAN, although in the UTLS PAN photolysis becomes the dominant loss process. Two minor loss processes of PAN are reaction with OH and dry deposition (Talukdar et al., 1995; Fischer et al., 2013). The major sources of NMVOCs are the emissions from fossil fuel and biofuel combustion and from industrial solvents (Tang et al., 2009). Biomass burning, biogenic and soil emissions also contribute to NMVOC and NOx production. Anthropogenic sources, of which alkanes are the most important class, are dominant in the extra tropical Northern Hemisphere outside the spring season. In spring, when surface PAN peaks, biogenic and anthropogenic NMVOCs species each support about 50% of the PAN burden. In the upper troposphere, lightning can add substantial amounts of NOx and thus lead to additional PAN production if NMVOC precursors are present, e.g. from convective uplifting from the boundary layer.

87 The estimated global NO_X production by lightning is ~3-5 Tg N/year (Schumann and
88 Huntrieser, 2007; Martin et al., 2007; Murray et al., 2012). Strong lightning activity during
89 ASM, NAM and WAM (Shepon, et al., 2007; Evett et al., 2008; Ranalkar and. Chaudhari, 2009;
90 Barret et al., 2010; Penki and Kamra, 2013) contributes to PAN production via lightning NO_X.
91 The estimated increase in PAN is ~20-30% due to nitrogen enhancement by lightning (Tie et al.,
92 2001).

93 Due to the cold temperatures in the UTLS, the chemical lifetime of PAN in this region is
94 several months. The PAN lifetime in ECHAM5-HAMMOZ simulations varies between 80 and
95 200 days in the tropical UTLS (figure not included). PAN therefore travels over long distances
96 and affects the NO_y partitioning in areas that are far away from the precursor emission regions.
97 Upon descent into warmer regions of the troposphere, PAN releases NOx which in turn increases
98 ozone and OH production in remote regions (Singh et al., 1986; Singh et al., 1998; Hudman et
99 al., 2004). PAN mixing ratios vary from less than 1 pptv in the remote marine atmosphere (as
100 observed during the NASA GTE PEM-Tropics B campaign in the South Pacific lower marine
101 boundary layer, data available at http://acd.ucar.edu/~emmons/DATACOMP/) to several ppbv in
102 the polluted urban environment and biomass burning plumes (Ridley et al., 1992; Singh et al.,
103 1998). In the UTLS mixing ratios are typically in the range 10-300 pptv (Emmons et al., 2000;
104 Keim et al., 2008).
105
106 To our knowledge, this is the first study that analyzes the influence of monsoon outflow
107 from different world regions on the distribution of peroxyacetyl nitrate (PAN) in the UTLS over
108 the Asian monsoon region, and its recirculation in the UTLS. We run decadal simulations with a
109 chemistry climate model and apply statistical comparisons with satellite and aircraft data,

thereby contributing to the objectives of the Chemistry Climate Model Initiative (CCMI, see http://www.igacproject.org/CCMI). The model climatology is evaluated with data from aircraft campaigns and the Michelson Interferometer for Passive Atmospheric Sounding (MIPAS) instrument onboard the ENVIronmental SATellite (ENVISAT). The transport of HNO_3 and NOx due to monsoon convection from different monsoon regions and the impacts of lightning on the UTLS trace gas distributions are analyzed from model simulations. The paper is organized as follows: Section 2 contains a short description of the data and model including the simulation setup. In sections 3, we discuss the various convective transport pathways of PAN into the UTLS, its redistribution in the stratosphere and its re-circulation across the various monsoon regions. The analysis of percentage changes in lightning produced ozone, HNO_3, PAN and NO_X on total concentrations over the convective zones is also presented. Conclusions are given in section 4.

2. Methods

2.1 Satellite measurements

The MIPAS–E instrument onboard the ENVISAT was launched in March 2002 into a polar orbit of 800 km altitude, with an orbital period of about 100 minutes and an orbit repeat cycle of 35 days. MIPAS–E (Fischer and Oelhaf, 1996; Fischer et al., 2008) was a Fourier Transform Spectrometer that provided continual limb emission measurements in the mid infrared over the range 685– 2410 cm−1 (14.6–4.15 μm). From June 2002 to March 2004 MIPAS-E operated in its full spectral resolution mode at an unapodized resolution of 0.035 cm^{-1}, and with tangent altitude steps of 3 km in the UTLS. From January 2005 through the end of the mission in April 2012 the spectral resolution was reduced to 0.0875 cm^{-1}, while the tangent altitude steps in the UTLS were reduced to 1.5 – 2 km. MIPAS-E monitored several atmospheric trace constituents affecting atmospheric chemistry including PAN, NO_X, and O_3. The details of the general retrieval method and setup, error estimates and use of averaging kernel and visibility flag are documented by Von Clarmann et al. (2009). In this study we analyze the MIPAS-E observed PAN data during the period 2002-2011. The data are available from http://share.lsdf.kit.edu/imk/asf/sat/mipas-export/Data_by_Target/. Details of the PAN retrievals, error budget, and vertical resolution are given by Glatthor et al. (2007) for the 2002 – 2004 measurement period for data version V3O_PAN_5, and by Wiegele et al. (2012) for the 2005 – 2012 measurement period for data version V5R_PAN_220/V5R_PAN_221 (different naming 220/221 merely due to technical reasons). The total error of PAN retrievals is below 20% from 10-12 km, below 30% from 12-16 km, and below 40% above 16km for V3O_PAN_5 (see Fig. 2 in Glatthor et al., 2007). The error is dominated by contributions of spectral noise and the uncertainty of the instrument pointing. Table 3 in Wiegele et al. (2012) indicates that for the

V5R_PAN_220/221 product the total error is below 10% from 10-12 km and above 100% for altitudes greater than 15 km. Again spectral noise and the uncertainty of the instrument pointing are the main contributors.

The sensitivity of the PAN retrievals can be judged by the averaging kernels. Since two types of retrievals are used in this study, V3O_PAN_5 and V5R_PAN_220/221 from high and reduced spectral resolution, respectively, we give two examples of the respective averaging kernel rows. The locations of the examples are 26 degree N and 81 degree E for the V3O_PAN_5 example and 28 degree N and 85 degree E for V5R_PAN_220. The figure S1 (a) and (b) shows the rows of the averaging kernels for an altitude range of 5 to 25 km. The diamonds indicate the respective nominal altitudes of the retrieval grid. The figure S1 shows that the retrieval results below 8-9 km are dominated by information from above the nominal altitude. A similar, albeit less obvious, situation develops for altitudes above 22-23 km. There and above the information has an increasing weight from lower than nominal altitudes. This is the reason why the MIPAS PAN data is not considered below 8 km and above 23 km. Another effect clearly visible in both example plots is that the altitude region which influences the retrieved PAN value at a given altitude is increasing with altitude, i.e. the vertical resolution decreases with altitude. To account for the comparatively low, and altitude dependent, vertical resolution, the model data to be directly compared to MIPAS measurements was convolved with the MIPAS PAN averaging kernel.

The data are contoured and gridded at 4 degree latitude and 8 degree longitude resolution. In the process the data quality specifications as documented at http://share.lsdf.kit.edu/imk/asf/sat/mipas-export/Documentation/ were employed, namely: only

data with visibility flag equal 1 and diagonal value of averaging kernel greater than 0.03 were used.

2.2 ECHAM5-HAMMOZ model simulation and experimental setup

The ECHAM5-HAMMOZ aerosol-chemistry-climate model used in the present study comprises of the general circulation model ECHAM5 (Roeckner et al., 2003), the tropospheric chemistry module, MOZ (Horowitz et al., 2003), and the aerosol module, Hamburg Aerosol Model (HAM) (Stier et al., 2005). It includes ozone, NO_X, VOC and aerosol chemistry. The gas phase chemistry scheme is based on the MOZART-2 model (Horowitz et al., 2003), which includes comprehensive Ox-NOx-hydrocarbons chemistry with 63 tracers and 168 reactions. The $O(^1D)$ quenching reaction rates were updated according to Sander et al. (2003), and isoprene nitrates chemistry according to Fiore et al. (2005). In the model simulations we included emissions of acetone from anthropogenic sources and wild fires (primary sources), while acetaldehyde and methylglyoxal are produced by oxidation of other NMVOCs (secondary sources). In particular, oxidation of primary NMVOCs like ethane (C_2H_6), propane (C_3H_8) and propene (C_3H_6) forms acetaldehyde, while CH_3COCHO is mainly formed from the oxidation products of isoprene and terpenes. Higher acyl peroxy nitrates (MPAN) are included in MOZART-2 chemical scheme, they are also formed through oxidation of NMVOCs, but their production is small compared to PAN. Thermal decomposition, and reaction with OH as well as the absorption cross sections for PAN photolysis are all specified according to Sander et al., 2003.

In ECHAM5-HAMMOZ dry deposition follows the scheme of Ganzeveld and Lelieveld (1995). Soluble trace gases such as HNO_3 and SO_2 are also subject to wet deposition. In-cloud and below cloud scavenging follows the scheme described by Stier et al. (2005). PAN is not highly water soluble, therefore dry and wet deposition are insignificant removal processes.

The model is run at a spectral resolution of T42 corresponding to about 2.8 x 2.8 degrees in the horizontal dimension and 31 vertical hybrid σ-p levels from the surface up to 10 hPa. We note that the nominal grid resolution of 2.8 degrees is somewhat misleading, because the spectral truncation of T42 only allows to resolve details on the order of 180/42 = 4.28 degrees. This is the main reason why we compare our model results with the MIPAS PAN retrievals on a 4 x 8 degree grid. The details of model parameterizations, emissions and validation are described by Pozzoli et al., (2008a,b, 2011) and Fadnavis et al. (2013).

The simulations were performed with varying monthly mean sea surface temperature (SST) and sea ice cover (SIC) data over the period 1995 – 2004 (AMIP). The simulations did not aim to exactly reproduce specific meteorological years, and we ran 10-year periods in order to obtain a reasonable statistics. We used the RETRO project data set of the year 2000 available at http://eccad.sedoo.fr/ for the surface CO, NO_x , and hydrocarbon emissions from anthropogenic sources and biomass burning (Schultz et al., 2004; 2005; 2007; 2008). Anthropogenic total RETRO emissions of the year 2000 are 476 Tg/year for CO and 90 Tg/year for NOx, 5 Tg/year of ethane, 3.5 Tg/year of propane and 2.7 Tg/year of propene, which are the main anthropogenic VOC precursors of PAN. Biomass burning RETRO emissions of year 2000 are 357 Tg/year for CO, and 16 Tg/year for NOx. 2.5 Tg/year for ethane, 1.3 Tg/year for propane, 2.7 Tg/year for propene, and 2.7 Tg/year for acetone. CO biomass burning emissions in southeast Asia account

212 for 7 Gg/month in spring, while up to 15 Gg/month were reported from Carmichael et al. [2003].
213 The anthropogenic and biomass burning emissions of SO_2 (total of 142 Tg/year), BC (7.7
214 Tg/year) and OC (66.1 Tg/year) are based on the AEROCOM emission inventory (Dentener et
215 al., 2006), also representative of the year 2000. The biogenic NMVOC emissions are calculated
216 on-line with the MEGAN module of Guenther et al. [2006]. The simulated global annual mean
217 emission of biogenic NMVOCs between 1995 and 2004 is 830 Tg(C)/year, isoprene contributes
218 by 57%, followed by terpenes (21%), methanol (12%), and other NMVOCs such as acetaldehyde
219 (2.5%) and acetone (2.3%). Other natural emissions calculated on-line by the model are the
220 Dimethyl Sulfide (DMS) fluxes (Kettle and Andreae, 2000; Nightingale et al., 2000; Pham et al.,
221 1995), sea salt aerosols (Schulz et al., 2004) from the oceans, and mineral dust aerosols (Tegen et
222 al., 2002; Cheng et al., 2008).

223 Our base year for aerosol and trace gas emissions is 2000, and emissions were repeated
224 annually throughout the simulation period. Lightning NOx emissions are parameterized
225 following Grewe et al. [2001]. They are proportional to the calculated flash frequency with a
226 production rate of 9 kg(N) per flash, and distributed vertically using a C-shaped profile. The
227 calculated flash frequency is resolution-dependent and scaled globally to yield annual global
228 emissions of 3.4 Tg(N) per year. To study the impact of lightning on the distributions of PAN
229 we compare two sets of experiments; each conducted for 10 years 1995-2004: (1) the control
230 experiment (CTRL) and (2) the lightning off experiment (light-off).

231 Model simulated PAN, NO_X, HNO_3 and Ozone mixing ratios are evaluated with
232 climatological datasets of airborne campaigns during the monsoon season (June-September). The
233 data were retrieved from http://acd.ucar.edu/~emmons/DATACOMP/CAMPAIGNS/ (see also

234 the paper by Emmons, 2000). The NO_X and ozone volume mixing ratios observed during
235 CAIPEEX experiment, September 2010, are evaluated over the Indian region. The details of
236 instruments and measurement techniques are available at
237 http://www.tropmet.res.in/~caipeex/about-data.php. The list of data sets and aircraft campaign
238 used for comparison are presented in Table 1. For the comparison, aircraft observations are
239 averaged over 0-2 km, 2-6 km and 6-8 km and horizontally over the coherent flight regions.

240 **3. Results and discussion**

241 **3.1 Comparison with aircraft measurements**

242 Figure 1(a)-(k) compare the observed global distribution of PAN, ozone, HNO_3 and NO_X to
243 those simulated by ECHAM5-HAMMOZ. The mean aircraft observations are shown as filled
244 circles and model output are background contours. Figure 1 indicates that model simulated PAN,
245 HNO_3 and NO_X show good agreement with aircraft measurements. Difference plots of PAN,
246 ozone, HNO_3 and NOx (ECHAM5-HAMMOZ-Aircraft observations) are shown in Figure S2 .
247 The model bias is different at each location. It varies with species and altitude. Between 0-2km,
248 simulated PAN shows positive bias ~7-12 ppt in the Western Pacific, 52-105 ppt over United
249 States of America (USA). Ozone shows positive bias ~7 ppb over India, ~3-15 ppb over western
250 Pacific, negative bias ~2-20 ppb in mid latitude Atlantic and positive bias 2-20 ppb over tropical
251 Atlantic, ~2-18 ppb over USA. HNO_3 is higher by ~20-75 ppt over Western pacific and less as ~-
252 5 ppt at few locations. Over the UAS bias is negative, less than 5 ppt. NOx shows positive bias
253 ~40 ppt over India and 0-10 ppt over the Western Pacific. Between 2-6km and 6-10km, over the
254 West Pacific simulated PAN show negative bias ~10-20 ppt and positive bias ~5-50 ppt at some
255 locations. Over the USA bias value are ~4-70 ppt. Ozone is lower by ~10-15 ppb and higher by

256 ~3-30 ppb at some locations in the western Pacific, 3-30 ppb over Atlantic and ~2-30 ppb over
257 USA. The positive bias in HNO_3 reduces to 3-20 ppt and negative bias to 3 to 20 ppt over the
258 Western Pacific, over the USA negative bias is ~20 ppt and positive bias is ~3-70 ppt. The NOX
259 shows negative bias ~40 ppt over India. The bias values vary between 6 to 10 ppt over Western
260 Pacific, 15 to -20 ppt over USA and Atlantic. As can be seen from above discussions, ozone
261 exhibits a low bias over South America and the Atlantic (for 0-6 km). Model simulated ozone
262 and NO_X show good agreement with CAIPEEX measurements over the Indian region.

263 **3.2 Comparison with MIPAS-E retrievals**

264 In order to study the influence of monsoon circulation on the distribution of PAN in the
265 UTLS region, seasonal mean (June-September) PAN concentrations are analyzed. Figures 2 (a)
266 and (b) present the seasonal mean distributions of the PAN retrievals from MIPAS-E averaged
267 over 14-16 km and for period 2002-2011. Simulated PAN concentrations by ECHAM5-
268 HAMMOZ are plotted in Figures 2 (b) for comparison. MIPAS-E observations (Figure 2(a))
269 show a maximum in PAN concentrations (~200-230 ppt) over (1) the Asian monsoon
270 anticyclone region (12-40N, 20-120E), and (2) over parts of North America, the Gulf Stream, (3)
271 southern Atlantic Ocean and west coast of tropical Africa. ECHAM5-HAMMOZ CTRL
272 simulations also show high PAN concentration at these locations (Fig. 2(b)), however PAN
273 concentrations are lower than MIPAS-E observations and appear somewhat more localized.
274 MIPAS-E exhibits a PAN maximum originating from African sources over the South Atlantic,
275 whereas the model shows this maximum over the African continent. This may be the outflow of
276 biomass burning over central and southern Africa during summer monsoon, which is
277 underestimated in the model. The biomass burning region of Africa is ~30S-20N; 20W-30E
278 (Glanter et al., 2000). The longitude-altitude and latitude-altitude cross-sections of MIPAS-E

observed and simulated PAN over the biomass burning region are plotted in figure S3. Model simulation shows that the biomass plume rising from Africa move westward and northward over the Atlantic Ocean and merges with South American plume. The difference between MIPAS observations and ECHAM5-HAMMOZ simulation plotted in figures S3 (c) and S3 (f). They show that the model underestimates biomass burning PAN by 20-60ppt. From satellite, aircraft observations and model simulations Real et al., (2010), Barret et al., (2008) reported a plume in the mid and upper troposphere over southern Atlantic which originates from central African biomass burning fire. These differences may also be related to issues in the vertical transport of PAN, or to a possible underestimate of the emission sources of non methane volatile organic compounds. Uncertainties in the rate coefficients and absorption cross sections of PAN may also play a role. Also anthropogenic NO_X emissions are mostly underestimated in the emission inventories (Miyazaki et al., 2012). As discussed in Fadnavis et al., 2014, UTLS PAN over the ASM is sensitive to NOx emission changes in India or China. In their study, also performed with ECHAM5-HAMMOZ, a 73% NOx emission change in India lead to a PAN increase of 10-18%, while a 73% NOx emission change in China changed PAN over the ASM by 18-30 % . The cross-section plots of (see figure S4) differences in MIPAS-E PAN with model simulated PAN indicate that in the UTLS (8-23km), MIPAS-E PAN is higher than model simulated PAN by ~20-60 ppt (except above 20km). It is lower by 20-40 ppt over eastern part of anticyclone (Southern India and South east Asia) and 20-40 ppt over Indonesia northern Australia. Near the southern pole MIPAS-E is PAN higher than ECHAM5-HAMMOZ by 20-90 ppt. The model could not produce high PAN concentrations near the southern pole between 17 and 23 km. In general, in the ASM region during the monsoon season MIPAS-E PAN is higher than model by

30-60 ppt between 8-16km and model bias vary between +40 ppt to -40 ppt between 17 and 23km.

3.3 Transport from Northern tropical land mass

From figures 2(a) it appears that air pollution is rising from Asia, North America and tropical Africa into the UTLS. Monsoon convective activity over Asia (June-September), North America (July-September) and tropical Africa (June-September, 10N-25^{O}S) appears to play a dominant role in vertical transport. Some fraction of this convective transport can reach the lower stratosphere (Park et al., 2009) and subsequent horizontal transport can redistribute PAN in the stratosphere.

To illustrate vertical transport, longitude-altitude cross sections of PAN mixing ratios averaged over the region 0-30°N and for June-September as obtained from MIPAS-E and ECHAM5-HAMMOZ are shown in Figures 3(a) and (b) respectively. Both MIPAS-E observations and ECHAM5-HAMMOZ simulations show elevated levels of PAN (200-250 ppt) near 80-100E (ASM), 30W-30E (WAM) and 80-100W (NAM) region. The simulated PAN distribution along with winds plotted in Figure 3(b) show cross tropopause transport from these regions. It reveals that transport of boundary layer PAN to UTLS mainly occurs from strong convective regions, mainly Bay of Bengal (~80-90E), South China Sea (~100-120E), western Atlantic Ocean (Gulf Stream region) and Gulf of Mexico (80-100W). MIPAS-E observations and model simulations show that the transport due to ASM is stronger and reaches deeper into the lower stratosphere. This is due to the more intense deep convection activity over the ASM region compared to the NAM region. Over the ASM region the MIPAS-E observations shows the PAN concentrations ~30-60 ppt near 20km while model simulations show it near 22km. Figure 3(c) illustrates longitude-altitude cross section of difference in MIPAS and model

simulated PAN. It appears that the model PAN is overestimated over the ASM (20-50 ppt) and underestimated over the NAM (50-70 ppt) and WAM (20-70 ppt) regions. However, the overestimation in the upper troposphere in the ASM is difficult to explain on physical grounds and is more likely to be a MIPAS-E sampling issue as discussed later.

3.4 Transport from southern tropical land mass

In order to understand transport of PAN due to southern WAM, SAM and AUSM, we consider longitude-pressure sections of MIPAS-E observations and model simulated PAN concentrations averaged over 0-25S. PAN concentrations from MIPAS-E and model simulations are plotted in figure 3(d)-(e) respectively. The model has plumes near 20E, 100E and 80W. These three regions of convective transport are (1) tropical southern Africa 10-40E, referred to as South Africa, (2) Indonesia and northern parts of Australia ~100-110E and (3) South America ~70-80W. Outflow from Indonesia and from northern parts of Australia (~100E) penetrates deeper into the UTLS. Tropical Rainfall Measuring Mission (TRMM) satellite observations show high frequency of intense overshooting convection over these areas (during the monsoon season) with highest density in the belt 0-10S over the Caribbean, Amazon, Congo and Southern Maritime Continent (Liu and Zipser, 2005). The analyses of vertical winds show strong transport from10-40E, 100-110E, 70-80W (in the belt 0-10S). The amount of high level cloud fraction is also high over these regions. The model simulations show high PAN concentrations reaching the UTLS. Thus transport due to deep convection is reasonably well captured by the model. However, the MIPAS-E observations only show a plume rising over South Africa, The AUSM (Indonesia-Australia) and SAM plumes are not distinguishable at these altitudes. Figure 3(e) shows that in the upper troposphere (8-14km) they are mixed by the prevailing westerly winds.

346 The reasons for a single plume seen in MIPAS-E may be that lower concentrations of PAN reach
347 these altitudes (above 8km) from SAM and AUSM and mix with the plume over South Africa.
348 Simulations shows less PAN concentrations over the longitudes of SAM and AUSM (see figure
349 3(e)). The differences between MIPAS observations and simulations (figure 3(f)) show that
350 model PAN is overestimated in the AUSM (20-50ppt) and is underestimated over the southern
351 WAM (20-70 ppt) and SAM (20-60 ppt) regions. It is likely that the three plume structure in the
352 upper troposphere seen in model is being obscured in the observations due to sampling issues
353 since periods of deep convection reaching significantly above 8 km are associated with
354 significant cloud cover.

355 Figure 3 shows that simulated transport of PAN due to ASM, NAM and WAM convection
356 are stronger and penetrate deeper into the upper troposphere compared to SAM and AUSM.
357 This is consistent with the distribution of deep convection noted by Gettelman et al. (2002). In
358 general, the PAN amounts in the UTLS in the model are less than observed by MIPAS-E. This
359 may be due to an underestimate of the chemical PAN source from VOC precursors or too little
360 vertical transport or a combination of both. Earlier model studies with ECHAM also exhibited
361 too low concentrations of CO in the upper tropospheric outflow (M. Schultz, unpublished data
362 from the NASA Global Tropospheric Experiment TRACE-P mission).

363 The area of low potential vorticity (PV) indicates the strength of the monsoon anticyclone
364 (Vaughan and Timmis, 1998; Pan etal., 2012; Garny and Randel, 2013). The analysis of model
365 simulated potential vorticity at 370K, shown in Figure 4 exhibits lower PV values over the ASM
366 region compared to the NAM, WAM, SAM and AUSM regions. This reflects a stronger
367 monsoon anticyclone over ASM. Out of all the regions in question convective activity is most

intense over the region spanning the southern flanks of the Himalayas and the Maritime Continent (e.g. Gettelman et al., 2002; see their Figure 3). The tropopause temperatures are typically the lowest in this region. Deep convection intensity is significant over Central America as well but is much more localized and not effective at pumping North American NOx emissions into the UTLS (see figure S5). Figure 4 shows a region of PV mixing in the southern hemisphere to the south of the ASM. This feature indicates the intensity of the near-equatorial convective heating in this region. The tropical heating drives an anticyclone pair circulation roughly symmetric around the equator (see Figure 1 of Park et al, 2007).

3.5 Transport from Asian Summer Monsoon region

The latitude-altitude sections over the ASM (60°-120°E) of MIPAS-E observed PAN (plotted in the altitude range 8-23 km) and ECHAM5-HAMMOZ CTRL simulations are shown in Figures 5(a) and (b), respectively. ECHAM5-HAMMOZ simulations are similar to MIPAS-E retrievals of PAN. There is indication of plume ascent into the lower stratosphere. The ECHAM5-HAMMOZ simulations also show transport of subtropical boundary layer PAN into the UTLS due to deep convection. This is not visible in the MIPAS-E data because of the lack of data below 8 km. Figure 5 (b) shows that there is transport from 40°-50°N reaching up to 10 km (~200 hPa). Park et al. (2004, 2007, 2009) and Randel and Park (2006) noted that trace species are introduced into the monsoon anticyclone at its eastern end around 200 hPa. The uplift over south-east Asia and the base of the Himalayas in India pumps tracers into the upper tropical troposphere where they get horizontally redistributed by the anticyclonic circulation and form the region of high PAN values between 40°N and high latitudes. Figure 8(c) shows that the mid-

latitude maximum seen in Figure 5(b) is due to pollution transport from Europe. The Chinese emissions are feeding into this large plume over Russia and partly being transported and diluted over the extratropical Pacific Ocean. The latitude-altitude section of difference between MIPAS and simulated PAN indicate that ASM plume is under estimated in the model (see figure 5 (c)). It is interesting to observe figure 3(c) (longitude –altitude section) and figure 5(c) (latitude-altitude section). The reason for underestimation of the ASM plume in the latitude-altitude section may be due to a lower contribution from the eastern part of anticyclone in the model. Figure S4 shows model PAN is underestimated over Southern India and South East Asia. Figure 5(c) indicates that the region of convective transport in the model around 30 N is narrower than observations. The model also underestimates PAN in the upper troposphere around 45 N. It is possible that the model is not capturing the observed structure of the large scale ASM circulation and its northern limit in the UTLS. The overestimation of PAN by the model in the northern middle and high latitudes in the UTLS (Figures 5(c, h, i)) is associated with European emissions and transport.

3.6 Transport from North American monsoon region

Figures 5(d) and (e) exhibit latitude-altitude sections of PAN from MIPAS-E retrievals and ECHAM5-HAMMOZ simulations (seasonal mean for July-September) over the North American monsoon region between 70W-120W. MIPAS-E observations and the model indicate transport of PAN into the UTLS. The distribution of ECHAM5-HAMMOZ simulated PAN from the boundary layer to UTLS shows the source region is at around 30N. There is convective uplift of PAN over the northern Gulf of Mexico region and over the Gulf Stream. High amount of pollutants are emitted from north east America from a number of power plants are located in Atlanta, Washington, Chicago, Boston, Jacksonville (CEC report, 2011). The tropospheric NO_2

columns retrieved from the SCIAMACHY and OMI satellite instrument shows high amount of anthropogenic NO_2 emissions over this region (Lamsal et al., 2011, Miyazaki et al., 2012). The model simulations show high amount of PAN concentrations over this region (see figures 8(a)-(d)). The monsoon convection lifts these pollutants to the upper troposphere. The outflow of these pollutants is over the Atlantic (see figures 2 (a)). TRMM precipitation radar observations show significant overshooting convective activity over this region during the monsoon season (Liu and Zipser, 2005). The vertical distribution of differences in MIPAS and simulated PAN shows that PAN is underestimated (see figure 5(f)) over the North and south America (10-60 ppt).

3.7 Transport from West African region

Figures 5(g)-(h) show vertical distributions of PAN over the African region (averaged over 0-45E). MIPAS-E observations and model simulations indicate a plume that crosses the tropopause and enters the lower stratosphere. The model surface fields (see Figure 5(h)) show that this plume arises from latitudes 5-20S over Africa and that it moves equatorward. It subsequently merges with the ASM plume. A prominent tongue of high PAN values between 30° and 60°N is captured in model simulations. This feature appears to be related to emissions from Europe being transported towards the equator in the upper subtropical troposphere. However, in the model, emissions from Europe, are transported poleward instead of equatorward (Figure 5(h)). There is a region of strong descent in the model between 30° and 40°N (see Figure 5(h)) which deforms the PAN isopleths around 12 km around 30°N downward. This feature is not seen in the MIPAS-E retrievals and indicates a disagreement of the model with the transport pattern of the atmosphere in this region. The transport of PAN in the 10-20°S latitude band over the Congo,

435 Angola, Tanzania regions of southern and tropical Africa is not pronounced in the model
436 compared to MIPAS-E observations. This behavior indicates that deep tropical convection is
437 underestimated in the model in this latitude band. The vertical distribution of differences in
438 MIPAS and simulated PAN (figure 5(i) shows that simulated PAN is underestimated over these
439 regions (5-20^{O}S and 20-40^{O}N).

440 The model simulated latitude-altitude, longitude-altitude cross sections of NO_X, and
441 HNO_3 over the ASM (10-40N, 60-120E), NAM (10-40N, 70-120W) and WAM (0-25S, 0-45E)
442 are shown in Figure 6 and 7. Figure 6 shows transport features in NOx. These are similar to those
443 seen in the distribution of PAN. This shows that monsoon convection lifts boundary layer
444 pollutants including NOy species to the UTLS. The distribution of HNO_3 (see Figure 7) shows a
445 complex pattern. Comparing Figure 3(b), the region around 100°E with intense convective uplift
446 corresponds to HNO_3 depletion from the surface to above 10 km. In fact, the upper troposphere
447 region of the ASM anticyclone exhibits much lower values of HNO_3 compared to all the other
448 longitudes in the 10-40°N band (Figure 7(c)). This suggests that in the model the convective
449 transport in the ASM region is associated with efficient removal by wet scavenging. In contrast,
450 the North American monsoon region has HNO_3 ascending to the upper troposphere with
451 significantly less loss. This is likely due to the fact that convection involved in vertical transport
452 during the NAM is not as intense and not as deep as in the case of the ASM and there are
453 differences in wet scavenging. Figure 7(b) shows that the plume rising from South America
454 moves towards the equator but does not have the extension into the upper troposphere as the
455 North American plume. These are June-September averages and the ITCZ is on the northern
456 hemisphere side during this period. Thus, weaker convective transport is to be expected on the
457 southern hemisphere side of the equator during this period. Figure 7 (d) shows significant

458 transport of African emissions around ~0-15S and a plume rising from Europe (~35-60°N) as
459 well.
460
461 **3.8 Horizontal transport**
462 PAN concentrations from MIPAS-E and ECHAM5-HAMMOZ simulations at different
463 altitudes are analyzed to understand horizontal transport. Figure 8(a) shows distribution of PAN
464 from ECHAM5-HAMMOZ simulations near the surface (2 km). Sources of PAN are apparent
465 over South America, southern Africa, North America, Europe, Russia and
466 northern China/Mongolia. The PAN distribution at 4 km (see Figure 8(b)) shows high
467 concentrations above these regions indicating vertical transport. Figures 8(c) and 8 (d) show the
468 distribution at 6 km and 8km. The upper level anticyclonic circulation between 10N and 30S
469 over the Atlantic transports PAN from central Africa towards America and from Brazil towards
470 southern Africa. The LBA-CLAIRE-98 campaign observations (Andreae et al., 2001) and
471 African Monsoon Multidisciplinary Analysis (AMMA) project (Real et al., 2010) show that the
472 biomass burning plume originating from Brazil is lifted to altitudes around 10km. This plume is
473 entrained into deep convection over the northern Amazon, transported out over the Atlantic and
474 then returned to South America by the circulation around a large upper-level anticyclone. This
475 transport is well captured by the model.
476 North American pollution is also being transported by the westerly winds over Eurasia,
477 forming an organized belt. This transport pattern persists up to 12km (Figure 8 (e) and 8(g)).
478 MIPAS-E observations at 12 km also show this transport pattern. The source region for the PAN
479 from southern Africa is the region of active biomass burning. Since this region is tropical, the
480 outflow is over the Atlantic due to the prevailing easterly zonal winds. ECHAM5-HAMMOZ

simulations shows similar transport (see Figures 8(g)). But there are differences; in particular the transport over tropical Africa does not get displaced over the Atlantic Ocean. As noted above, there are significant transport differences between the model and observations in this longitude band. Another difference is that PAN is not transported westward over Central America and towards the Pacific Ocean.

Figures 8(f)-8(h) show the distribution of PAN from MIPAS-E retrievals and ECHAM5-HAMMOZ simulations, in the lower stratosphere (18km). In both data sets PAN is transported westwards from ASM, NAM and WAM by prevailing easterly winds.

As can be seen from the above discussions, the ASM, NAM, and WAM outflow and convection over the Gulf Stream play an important role in the transport of boundary layer pollution into the UTLS. Previous studies (e.g. Fadnavis et al., 2013) indicate that over the Asian monsoon region, transport into the lower stratosphere occurs and there is significant vertical transport over the southern slopes of the Himalayas (Fu et al., 2006, Fadnavis et al., 2013) and also over the region spanned by the Bay of Bengal and the South China Sea (Park et al., 2009). Pollutant transport due to North American convection and tropical African outflow does not penetrate as deep into the stratosphere as the ASM. However there is clear indication that in the upper troposphere, middle latitude westerly winds connect the North American pollution to the ASM.

Figures 2-5 show that in the upper troposphere, westerly winds drive North American and European pollutants eastward to at least partly merge with the ASM plume. Strong ASM convection transports these remote and regional pollutants into the stratosphere. The Caribbean is a secondary source of pollutant transport into the stratosphere. In the stratosphere the injected

503 pollutants are transported westward by easterly winds and into the southern subtropics by the
504 Brewer-Dobson circulation.
505
506 **3.9 Impact of Lightning on tropospheric PAN, NO_X, HNO_3 and ozone**
507 Long-range transport of PAN may increase NO_X and hence ozone concentrations at
508 remote locations. In the tropical lower troposphere, NO_X is rapidly converted into HNO_3 due to
509 high amounts of OH. During the monsoon season the NOx released from intense lightning
510 activity enhances the formation of PAN, HNO_3 and ozone which is already relatively strong due
511 to the intense solar radiation along with high background concentrations of NOx, HOx and
512 NMVOCs in the ASM region (Tie et al., 2001). The percentage change in ozone, HNO_3, PAN
513 and NO_X due to lightning is computed from the difference between the control and lightning-off
514 experiments. We analyze the regional impacts of the lightning source at mid-tropospheric and
515 upper tropospheric pressure levels. Figure 9(a)-(d) shows the respective changes in the zonally
516 averaged spatial distribution of seasonal mean (June-September) ozone, HNO_3, PAN and NO_X
517 mixing ratios due to lightning. The analysis indicates that the impact of lightning on these
518 species is largest in the tropical upper troposphere. The enhancement takes place between 40^0N-
519 40^0S and between 8 km and 14 km. In the tropical mid troposphere lightning produced maximum
520 ozone is ~15-25%, HNO_3 ~ 40-60% ~ PAN ~15-25% and NO_X ~20-40% while in the upper
521 troposphere ozone is ~20-30%, HNO_3 ~60-75%, PAN ~28-35%, and NOx ~50-75%. Our results
522 are consistent with, albeit slightly lower than MOZART model simulations by Tie et al., (2001)
523 who show that lightning enhances PAN formation by 20-30%, NO_X ~50% and HNO_3 by 60-
524 80% in the middle troposphere. Labrador et al. (2005) also reported similar results from
525 simulations using the Model of Atmospheric Transport and Chemistry Max-Planck-Institute

526 (MATCH-MPI). The spatial distributions of NO_X, ozone, and PAN and HNO_3 produced from
527 lightning (see figures 9 (e) – 8(h)) indicate that in the upper troposphere (12km) increase in O_3
528 ~20-25% (11-17 ppbv), HNO_3 ~40-70%, PAN ~25-35 % and NO_X ~55-75%, over North
529 America are in agreement with previous studies (e.g Labrador et al., 2005; Hudman et al. 2007;
530 Zhao et al., 2009; Cooper et al., 2009), over equatorial Africa (PAN 30-45%, HNO3 ~70-80%
531 O3 ~ 25%, NOx~70%) agrees well with Barret et al., 2010; Bouarar et al., 2011 and over the
532 ASM region (PAN ~ 25%, HNO_3 ~65-70%, O3~ 20%, NOx ~ 60-70%) agrees with Tie et al.,
533 (2001). These regions coincide with regions of convective vertical transport of PAN (as seen in
534 figures 3 and 5). PAN will be lifted into the lower stratosphere by the monsoon convection along
535 with anthropogenic emissions and will redistribute in the tropical lower stratosphere. Latitude-
536 longitude cross sections of lightning induced PAN, NO_X, ozone and HNO_3 formation at altitudes
537 between 8-14km show that the production of PAN, NO_X, ozone and HNO_3 is less over the ASM
538 region than over the equatorial Americas and Africa (also seen in figure 9). The high amounts of
539 PAN over the ASM (see figures 2, 3, 5) are therefore primarily due to anthropogenic emission
540 transport into the UTLS from the source regions in Southern and Eastern Asia.

541

4. Conclusions

This study presented a statistical analysis of global decadal PAN observations from the MIPAS instrument on the Envisat satellite for the period 2002-2011 and ECHAM5-HAMMOZ global model simulations. The model and the observations, show that pollution outflow from the Asian summer monsoon (ASM), the North American Monsoon (NAM) and the West African monsoon (WAM) regions penetrates into the UTLS during the monsoon season. Uplifting due to ASM convection is deeper than in the NAM and WAM regions during the June-September period. In the upper troposphere, westerly winds drive North American and northward propagating South African pollutants eastward where they mix with the ASM plume. Deep, overshooting convection and strong diabatic upwelling in the ASM convection transports a part of these plumes into the lower stratosphere. The Caribbean region is another source of pollution transport into the stratosphere. Some cross tropopause transport occurs due to overshooting convection over North America and Southern Africa as well. In the lower stratosphere the injected pollutants from ASM, WAM and NAM are transported westward by easterly winds and into the southern hemisphere subtropics by the Brewer-Dobson circulation. In the southern hemisphere, plumes rising from convective zones of South Africa, South America and Indonesia-Australia are evident in the model simulations, but are not seen in the MIPAS retrievals. PAN concentrations are higher in the plume rising from South Africa than SAM and AUSM. In the upper troposphere, they merge by the prevailing westerly winds. MIPAS-E observations in the UTLS show a single plume over South Africa and no enhancement over SAM or AUSM. The reasons for the single plume seen in MIPAS-E may be that although there is uplifting by

each of the three monsoon systems lower concentrations of PAN reach these altitudes (above 8km) from SAM and AUSM until they merge with South African plume. It is also possible that the three plume structure in the upper troposphere seen in the model is being obscured in the observations due to sampling issues. Convective cloud cover is strongly associated with deep convection in the ASM region. The MIPAS-E data has a PAN minimum in the upper troposphere right in the longitude band of the deep convection over the southern flanks of the Himalayas (Figure 3(a)). This feature is unphysical and clearly identifies a sampling bias. However, the model is also not fully reproducing the latitudinal structure of the PAN in the ASM region UTLS which indicates that there are differences in both the distribution of convection and the large scale circulation.

The horizontal transport of PAN analyzed from ECHAM5–HAMMOZ simulations shows that the PAN from southern Africa and Brazil is transported towards America by the circulation around a large upper-level anticyclone and then lifted to the UTLS in the NAM region.

The vertical distribution of simulated HNO_3 over the monsoon regimes shows its depletion from the surface to 10 km at the foothills of the Himalayas. In contrast, the results show strong uplifting of HNO_3 into the upper troposphere with NAM convection. This may be due to the fact that NAM convection is not as intense as the ASM and there may be more wet removal of nitrogen oxides in the ASM convection. The model simulations indicate a higher efficiency of NOx conversion to HNO_3 over the Indian region compared to NAM.

Lightning production of NO_x may enhance PAN concentrations in the upper troposphere and affect its transport into the lower stratosphere. The percentage change in lightning produced ozone, HNO_3, PAN and NO_X has been evaluated with a sensitivity simulation. In the upper

586 troposphere, lightning causes significant increases in these species over equatorial America,
587 equatorial Africa and the ASM region. These regions coincide with intense convective zones
588 with significant vertical transport. Lighting production is higher over equatorial Africa and
589 America compared to the ASM. However, the vertical distribution shows that higher amounts of
590 PAN are transported into the upper troposphere in the ASM region. This indicates that the
591 dominant contribution to PAN over the ASM is from anthropogenic emissions. This is consistent
592 with the fact that anthropogenic emissions in the ASM region are higher than in the NAM and
593 WAM (Lamsal et al., 2011, Miyazak et al., 2012).

594 Recent observations show a positive trend (with time) in lightning (Price and Asfur,
595 2006) and deep convective activity over the tropical land mass (Aumann and Ruzmaikin, 2013).
596 TRMM precipitation radar also shows high density of deep overshooting events over the
597 convective regions of the Caribbean, Mexico, Sahara desert, Congo and Indonesia (Liu and
598 Zipser, 2005) during the summer monsoon season. This should amplify the UTLS trend from
599 increasing tropospheric pollution. However, an analysis of this process is beyond the scope of
600 this study.

601

602 *Acknowledgements*: The authors thank the MIPAS-E teams for providing data and the High
603 Power Computing Centre (HPC) in IITM, Pune, India, for providing computer resources.

604

605 References

606 Andreae, M. O., Artaxo, P., Fischer, H., Freitas, S. R., Grégoire, J.-M., Hansel, A., Hoor, P.,
607 Kormann, R., Krejci, R., Lange, L., Lelieveld, J., Lindinger, W., Longo, K., Peters, W.,
608 de Reus, M., Scheeren, B., Silva Dias, M. A. F., Ström, J., Velthoven, P. F. J. van and
609 William, J.: Transport of biomass burning smoke to the upper troposphere by deep
610 convection in the equatorial region, Geophy.,Res. Lett., 28, 951-958, 2001.

611 Aumann, H. H. and Ruzmaikin, A.: Frequency of deep convective clouds in the tropical zone
612 from 10 years of AIRS data, Atmos. Chem. Phys., 13, 10795–10806, 2013.

613 Barret, B., Williams, J. E., Bouarar, I., Yang, X., Josse, B., Law, K., Pham, M., Flochmoen, E.
614 Le, Liousse, C., Peuch, V.H., Calver, G.D., Pyle, J.A., Sauvage ,B., Velthoven P. van and
615 Schlager, H.: Impact of West African Monsoon convective transport and lightning NOx
616 production upon the upper tropospheric composition: a multi-model study, Atm. Chem.
617 Phys., **10**, 5719-5738, doi:10.5194/acp-10-5719-2010, 2010.

618 Barret B., Ricaud P., Mari C., Attie´ J.-L., Bousserez N., Josse B., Flochmoen E. LeLivesey N.
619 J., Massart S., Peuch V.-H., , Piacentini A., Sauvage B., Thouret V., and Cammas J.-P.
620 Transport pathways of CO in the African upper troposphere during the monsoon season:
621 a study based upon the assimilation of spaceborne observations, Atmos. Chem. Phys., 8,
622 3231–3246, 2008.

623 Barth, M., Lee, C, J., Hodzic, A. Pfister, G., Skamarock, W. C., Worden, J. , Wong, J., and
624 Noone, D.: Thunderstorms and upper troposphere chemistry during the early stages of the
625 2006 North American Monsoon, Atmos. Chem. Phys., 12, 11003–11026, 2012.

626 Bouarar, I., Law, K. S., Pham, M., Liousse, C., Schlager, H., Hamburger, T., Reeves, C. E.,
627 Cammas, J.-P., Ned´ el´ ec´ P., Szopa, S, Ravegnani, F., Viciani, S., D'Amato F.,

628 Ulanovsky A., and Richter A.: Emission sources contributing to tropospheric ozone over
629 Equatorial Africa during the summer monsoon, Atmos. Chem. Phys., 11, 13395–13419,
630 doi:10.5194/acp-11-13395-2011, 2011.
631 Carmichael, G. R., Tang Y., Kurata G., Uno I., Streets D., Woo J.-H.,
632 Huang H., Yienger J., Lefer B., Shetter R., Blake D., Atlas E., Fried
633 A., Apel E., Eisele F., Cantrell C., Avery M., Barrick J., Sachse G.,
634 Brune W., Sandholm S., Kondo Y., Singh H., Talbot R., Bandy A.,
635 Thorton D., Clarke A., and Heikes B., Regional-scale chemical
636 transport modeling in support of the analysis of observations obtained
637 during the TRACE-P experiment, J. Geophys. Res., 108(D21), 8823,
638 doi:10.1029/2002JD003117, 2003
639 CEC (Commission for Environmental Cooperation) report on North American Power Plant Air
640 Emissions, IBSN : 978-2-89700-008-0,October 2011.
641 Chang, Chih-Pei, Ding Y., Lau, Gabriel Ngar-Cheung, Johnson, R. H, Wang, B., and Yasunari,
642 T.: The Global Monsoon System: Research and Forecast (2nd Edition) edited by Chih-
643 Pei Chang et al., World Scientific Publishing Co, 2011.
644 Choi, Y., Kim, J., Eldering, A., Osterman, G., Yung, Y. L., Gu, Y., and Liou, K. N.: Lightning
645 and anthropogenic NOx sources over the United States and the western North Atlantic
646 Ocean: impact on OLR and radiative effects, Geophys. Res. Lett., 36, L17806,
647 doi:10.1029/2009GL039381, 2009.
648 Collier J.C. and Zhang G.J.: Simulation of the North American Monsoon by the NCAR CCM3
649 and Its Sensitivity to Convection Parameterization, J. of Clim., 2851-2866, 2006.

650 Cooper, O. R., Eckhardt, S., Crawford, J. H., Brown, C. C., Cohen, R. C., Bertram, T. H.,
651 Wooldridge, P., Perring, A., Brune, W.H., Ren, X., Brunner, D., and Baughcum, S. L.:
652 Summertime buildup and decay of lightning NOx and aged thunderstorm outflow above
653 North America, J. Geophys.Res., 114, D01101, doi:10.1029/2008JD010293, 2009.
654 Dickerson, R. R., Huffman, G. J., Luke, W. T., Nunnermacker, L. J., Pickering, K. E. , Leslie,
655 A., Lindsey, C., Slinn, W., Kelly, T., Daum, P., Delany, A., Grennberg, J., Zimmerman,
656 P., Boatman, J., Ray, J., and Stedman, D.: Thunderstorms: An important mechanism in
657 the transport of air pollutants, Science, 235, 460 – 465, 1987.
658 Dong, L. and Colucci, S. J. : The Role of Deformation and Potential Vorticity in Southern
659 Hemisphere Blocking Onsets, J. Atmos. Sci., 62, 4043-4056, 2005.
660 Drummond, J. W., D. H. Ehhalt, and A. Volz, Measurements of nitric oxide between 0 – 12
661 km altitude and 67 N-60 S latitude obtained during STRATOZ III, J. Geophys. Res,
662 93, 15,831 – 15,849, 1988.
663 Emmons, L. K., Hauglustaine, D. A., Muller, J.-F., Carroll, M. A., Brasseur, G. P., Brunner, D.,
664 Staehelin, J., Thouret, V., and Marenco, A.: Data composites of tropospheric ozone and
665 its precursors from aircraft measurements, J. Geophys. Res., 105, 20,497 – 20,538, 2000.
666 Evett, R. R., Mohrle C. R., Hall B. L., Brownb T. J. and Stephens S. L.: The effect of monsoonal
667 atmospheric moisture on lightning fire ignitions in southwestern North America,
668 Agricultural and forest meteorology, 148, 1478–1487, 2008.
669 Fadnavis, S., Semeniuk, K., Pozzoli, L., Schultz, M. G., Ghude, S. D., Das, S. and Kakatkar, R.:
670 Transport of aerosols into the UTLS and their impact on the Asian monsoon region as
671 seen in a global model simulation, Atmos. Chem. Phys., 13, 8771–8786, 2013,
672 doi:10.5194/acp-13-8771-2013.

673 Fadnavis S, Schultz M. G., Semeniuk K., Mahajan A. S., Pozzoli L., Sonbawne S., Ghude S. D.,
674 Kiefer M., and Eckert E., Trends in Peroxyacetyl Nitrate (PAN) in the Upper
675 Troposphere and Lower Stratosphere over Southern Asia during the summer monsoon
676 season: Regional Impacts, Atmos. Chem. Phys. Discuss., 14, 19055–19094,
677 doi:10.5194/acpd-14-19055-2014, 2014 (accepted for publication in ACP).
678 Fiore, A. M., Horowitz, L. W., Purves, D. W., Levy II, H., Evans, M. J., Wang, Y., Li, Q., and
679 Yantosca, R. M.: Evaluating the contribution of changes in isoprene emissions to surface
680 ozone trends over the eastern United States, J. Geophys. Res., 110, D12303,
681 doi:10.1029/2004JD005485, 2005.
682 Fischer E. V., Jacob D. J., Yantosca R. M., Sulprizio M. P., Millet D. B., Mao J., Paulot F.,
683 Singh H. B., Roiger A., Ries L., Talbot R.W., Dzepina K., and Pandey Deolal S.,
684 Atmospheric peroxyacetyl nitrate (PAN): a global budget and source attribution, Atmos.
685 Chem. Phys., 14, 2679–2698, doi:10.5194/acp-14-2679-2014, 2014.
686 Fischer, E. V., Jacob, D. J., Yantosca, R. M., Sulprizio, M. P., Millet, D. B., Mao, J., Paulot, F.,
687 Singh, H. B., Roiger, A.-E., Ries, L., Talbot, R. W., Dzepina, K., and Pandey Deolal, S.:
688 Atmospheric peroxyacetyl nitrate (PAN): a global budget and source attribution, Atmos.
689 Chem. Phys. Discuss., 13, 26841–26891, 2013.
690 Fischer, H. and Oelhaf, H.: Remote sensing of vertical profiles of atmospheric trace constituents
691 with MIPAS limb-emission spectrometers, Appl. Optics, 35, 2787–2796, 1996.
692 Fischer, H., Birk, M., Blom, C., Carli, B., Carlotti, M., von Clarmann, T., Delbouille, L., Dudhia,
693 A., Ehhalt, D., Endemann, M., Flaud, J. M., Gessner, R., Kleinert, A., Koopman, R.,
694 Langen, J., Lopez-Puertas, M., Mosner, P., Nett, H., Oelhaf, H., Perron, G., Remedios, J.,
695 Ridolfi, M., Stiller, G., and Zander, R.: MIPAS: an instrument for atmospheric and

climate research, Atmos. Chem. Phys., 8, 2151–2188, 2008, doi:10.5194/acp-8-2151-2008.

Fu, R., Hu, Y., Wright, J. S., Jiang, J. H., Dickinson, R. E., Chen, M., Filipiak, M., Read, W. G., Waters, J.W. and Wu, D. L.: Short circuit of water vapour and polluted air to the global stratosphere by convective transport over the Tibetan Plateau, Proc Natl Acad Sci U S A. Apr 11, 103(15), 5664-9, Epub Apr 3, 2006.

Galanter, M., H. Levy II, and G. R. Carmichael (2000), Impacts of biomass burning on tropospheric CO, NO_x, and O_3, J. Geophys. Res., 105(D5), 6633–6653, doi:10.1029/1999JD901113.

Ganzeveld, L., and Lelieveld, J.: Dry deposition parameterization in a chemistry general circulation model and its influence on the distribution of reactive trace gases, J. Geophys. Res.,100(D10), 20999–21012, doi:10.1029/95JD02266, 1995.

Garny, H., and Randel, W. J.: Dynamic variability of the Asian monsoon anticyclone observed in potential vorticity and correlations with tracer distributions, J. Geophys. Res. Atmos., 118, 13,421–13,433, doi:10.1002/2013JD020908, 2013.

Gettelman, A., Salby, M. L., and Sassi, F.: Distribution and influence of convection in the tropical tropopause region, J. Geophys. Res., 107(D10), 4080, doi:10.1029/2001JD001048, 2002.

Glatthor, N., Clarmann, T. von, Fischer, H., Funke, B., Grabowski, U., Höpfner, M., Kellmann, S., Kiefer, M., Linden, A., Milz M., Steck, T., and Stiller, G.P.: Global peroxyacetyl nitrate (PAN) retrieval in the upper troposphere from limb emission spectra of the Michelson Interferometer for Passive Atmospheric Sounding (MIPAS), Atmos. Chem. Phys., 7, 2775-2787, www.atmos-chem-phys.net/7/2775/2007/ doi:10.5194/acp-7-2775-2007, 2007.

Grewe, V., Brunner, D., Dameris, M. , Grenfell, J.L., Hein, R., Shindell, D. and Staehelin, J. : Origin and Variability of Upper Tropospheric Nitrogen Oxides and Ozone at Northern Mid-Latitudes. Atmos. Environ., 35, 3421-3433, 2001.

723 Harris, R. C., et al., The Amazon boundary layer experiment (ABLE 2A) dry season 1985, J.
724 GeOphys. Res., 93, 1351-1360, 1988.

725 Harriss, R.C., S.C. Wofsy, D.S. Bartlett, M.C. Shipham, D.J. Jacob, J.M. Hoell, Jr., R.J.
726 Bendura, J.W. Drewry, R.J. McNeal, R.L. Navarro, R.N. Gidge, and V.E. Rabine, The
727 Arctic Boundary Layer Expedition (ABLE 3A): July-August 1988, J. Geophys. Res., 97,
728 16,383-16,394, 1992.

729 Harriss, R.C., S.C. Wofsy, J.M. Hoell, Jr., R.J. Bendura, J.W. Drewry, R.J. McNeal, D. Pierce,
730 V.Rabine, and R.L. Snell, The Arctic Boundary Layer Expedition (ABLE-3B): July-
731 August 1990, J. Geophys. Res., 99, 1635-1643, 1994.

732 Hassim, M. E. E., Lane, T. P., and May, P. T.: Ground-based observations of overshooting
733 convection during the Tropical Warm Pool-International Cloud Experiment, J. Geophys.
734 Res. Atmos.,119, 880–905, doi:10.1002/2013JD020673, 2014.

735 Hoell, J. M., Jr., D. L. Albritton, G. L. Gregory, R. J. McNeal, S. M. Beck, R. J. Bendura, and J.
736 W. Drewry, Operational overview of NASA GTE/CITE 2 airborne
737 instrumentintercomparisons: Nitrogen dioxide, nitric acid, and peroxyacetyl nitrate, J.
738 Geophy. Res., 95, 10,047-10,054, 1990.

739 Hoell, J. M., Jr., D. L. Albritton, G. L. Gregory, R. L. McNeal, S. M. Beck, R. J. Bendura, and J,
740 W. Drewry, Operational overview of NASA GTE/CITE-2 airborne instrument
741 intercomparison: Nitrogen dioxide, nitric acid, and peroxyacetyl nitrate. *J. Geophy.*
742 *Res*., *95*, 10,047-10,054, 1990

743 Horowitz, L. W., Walters, S., Mauzerall, D. L., Emmons, L. K., Rasch, P. J., Granier, C., Tie, X.,
744 Lamarque, J., Schultz, M. G.,Tyndall, G. S., Orlando, J. J. and Brasseur, G. P.: A global
745 simulation of tropospheric ozone and related tracers, Description and evaluation of
746 MOZART, version 2, J. Geophys. Res.,108(D24), 2003.

747 Hudman, R. C., Jacob, D. J., Cooper, O. R., Evans, M. J., Heald, C. L., Park, R. J., Fehsenfeld,

748 F., Flocke, F., Holloway, J., Hübler, G., Kita, K., Koike, M., Kondo, Y., Neuman, A.,

749 Nowak, J., Oltmans, S., Parrish, D., Roberts, J. M., and Ryerson, T.: Ozone production in

transpacific Asian pollution plumes and implica tions for ozone air quality in California, J. Geophys. Res., 109, D23S10, doi:10.1029/2004jd004974, 2004.

Hudman, R. C., Jacob, D. J., Turquety, S., Leibensperger, E. M., Murray, L. T., Wu, S., Gilliland, A. B., Avery, M., Bertram,T. H., Brune, W., Cohen, R. C., Dibb, J. E., Flocke, F. M.,Fried, A., Holloway, J., Neuman, J. A., Orville, R., Perring, A.,Ren, X., Ryerson, T. B., Sachse, G. W., Singh, H. B., Swanson, A., and Wooldridge, P. J.: Surface and lightning sources of nitrogen oxides over the United States: magnitudes, chemical evolution, and outflow, J. Geophys. Res., 112, D12S05, doi:10.1029/2006JD007912, 2007.

Keim, C., Liu, G. Y. , Blom, C.E., Fischer, H., Gulde, T., Höpfner, M., Piesch, C., Ravegnani, F., Roiger, A., Schlager, H., and Sitnikov, N.: Vertical profile of peroxyacetyl nitrate (PAN) from MIPAS-STR measurements over Brazil in February 2005 and its contribution to tropical UT NO_y partitioning, Atmos. Chem. Phys., 8, 4891-4902, doi:10.5194/acp-8-4891-2008, 2008.

Khaykin S., Pommereau, J.-P., Korshunov, L., Yushkov, V., Nielsen, J., Larsen, N., Christensen, T., Garnier, A., Lukyanov, A., and Williams, E.: Hydration of the lower stratosphere by ice crystal geysers over land convective systems, Atmos. Chem. Phys., 9, 2275–2287, 2009.

Labrador, L. J., Kuhlmann, R. von, and Lawrence, M. G.: The effects of lightning-produced NOx and its vertical distribution on atmospheric chemistry: sensitivity simulations with MATCH-MPIC, Atmos. Chem. Phys., 5, 1815–1834, 2005.

Lamsal, L. N., Martin, R. V., Padmanabhan, A., van Donkelaar, A., Zhang, Q., Sioris, C. E., Chance, K., Kurosu, T. P., and Newchurch, M. J.: Application of satellite observations for timely updates to global anthropogenic NOx emission inventories, Geophys. Res. Lett., 38,L05810, doi:10.1029/2010GL046476, 2011.

775 Li, Q., Jiang, J. H., Wu, D. L., Read, W. G., Livesey, N. J., Waters, J. W., Zhang, Y., Wang, B.,
776 Filipiak, M. J., Davis, C. P., Turquety, S., Wu, S., Park R. J., Yantosca R. M., and Jacob
777 D. J.: Convective outflow of South Asian pollution: A global CTM simulation compared
778 with EOS MLS observations, Geophys. Res. Lett., 32, L14826,
779 doi:10.1029/2005GL022762, 2005.

780 Liu, C., and Zipser E. J.: Global distribution of convection penetrating the tropical tropopause, J.
781 Geophys. Res., 110, D23104, 2005.

782 Martin, R. V., Sauvage, B., Folkins, I., Sioris, C. E., Boone, C., Bernath, P., and Ziemke, J.:
783 Space-based constraints on the production of nitric oxide by lightning, J. Geophys. Res.,
784 112, D09309, doi:10.1029/2006JD007831, 2007.

785 Miyazaki, K., Eskes, H. J., and Sudo, K.: Global NOx emission estimates derived from an
786 assimilation of OMI tropospheric NO2 columns, Atmos. Chem. Phys., 12, 2263–2288,
787 doi:10.5194/acp-12-2263-2012, 2012.

788 Murray, L. T., Jacob, D. J., Logan, J. A., Hudman, R. C., and Koshak, W. J.: Optimized regional
789 and interannual variability of lightning in a global chemical transport model constrained
790 by LIS/OTD satellite data, J. Geophys. Res., 117, D20307, doi:10.1029/2012JD017934,
791 2012.

792 O'Sullivan D. W., • Heikes B. GLee., M., Chang W., Gregory G. L., • Blake D. R., and Sachs
793 G. W., Distribution of hydrogen peroxide and methylhydroperoxide over the Pacific and
794 South Atlantic Oceans, *J. Geophys. Res*, 104, D5, 5635-5646, 1999.

795 L. L. Pan1 , A. Kunz1,*, C. R. Homeyer2 , L. A. Munchak1,**, D. E. Kinnison1 , and S. Tilmes,
796 Commentary on using equivalent latitude in the upper troposphere and lower
797 stratosphere, Atmos. Chem. Phys., 12, 9187–9199, doi:10.5194/acp-12-9187-2012 ,
798 2012,

799 Park M., Randel W. J., Getteleman, A., Massie, S. T., and Jiang, J. H.: Transport above the
800 Asian summer monsoon anticyclone inferred from Aura Microwave Limb Sounder
801 tracers, J. Geophys. Res., 112, D16309, doi:10.1029/2006JD008294, 2007.
802 Park, M., Randel, W. J., Emmons, L. K., and Livesey, N. J.: Transport pathways of carbon
803 monoxide in the Asian summer monsoon diagnosed from Model of Ozone and Related
804 Tracers (MOZART), J. Geophys. Res., 114, D08303, doi:10.1029/2008JD010621, 2009.
805 Park, M., Randel, W. J., Kinnison, D. E., Garcia, R. R., and Choi, W.: Seasonal variation of
806 methane, water vapour, and nitrogen oxides near the tropopause: Satellite observations
807 and model simulations, J. Geophys. Res., doi:10.1029/2003JD003706, 109, D03302,
808 2004.
809 Penki, R. K. and Kamra, A. K.: Lightning distribution with respect to the monsoon trough
810 position during the Indian summer monsoon season, J. Geophy. Res., 118, 4780–4787,
811 doi:10.1002/jgrd.50382, 2013.
812 Pozzoli, L., Bey, I., Rast, J. S., Schultz, M. G., Stier, P., and Feichter, J.: Trace gas and aerosol
813 interactions in the fully coupled model of aerosol-chemistry-climate ECHAM5-
814 HAMMOZ: 1. Model description and insights from the spring 2001 TRACE-P
815 experiment, J. Geophys. Res., 113, D07308, doi:10.1029/2007JD009007, 2008a.
816 Pozzoli, L., Bey, I., Rast, J. S., Schultz, M. G., Stier, P., and Feichter, J.: Trace gas and aerosol
817 interactions in the fully coupled model of aerosol-chemistry-climate ECHAM5-
818 HAMMOZ: 2. Impact of heterogeneous chemistry on the global aerosol distributions, J.
819 Geophys. Res., 113, D07309, doi:10.1029/2007JD009008, 2008b.
820 Pozzoli, L., Janssens-Maenhout, G., Diehl, T., Bey, I., Schultz, M. G., Feichter, J., Vignati, E.,
821 and Dentener, F.: Re-analysis of tropospheric sulfate aerosol and ozone for the period
822 1980–2005 using the aerosol-chemistry-climate model ECHAM5-HAMMOZ, Atmos.
823 Chem. Phys., 11, 9563-9594, doi:10.5194/acp-11-9563-2011, 2011.
824 Prabha T.V., Khain A., Maheshkumar R.S., Pandithurai G., Kulkarni J.R., Goswami B.N.
825 (2011),Microphysics of Premonsoon and Monsoon Clouds as Seen from In Situ
826 Measurements during the Cloud Aerosol Interaction and Precipitation Enhancement

827 Experiment (CAIPEEX), **J. Atm. Sc.**, Vol.68 , 2011, DOI: 10.1175/2011JAS3707.1,
828 1882-1901

829 Price, C. and Asfur, M.: Inferred long term trends in lightning activity over Africa, Earth Planets
830 Space, 58, 1197–1201, 2006.

831 Ranalkar, M. R and Chaudhari, H. S.**:** Seasonal variation of lightning activity over the Indian
832 subcontinent. *Meteorology and Atmospheric Physics*. 104, 125–134, 2009.

833 Randel, W. J. and Park, M.: Deep convective influence on the Asian summer monsoon
834 anticyclone and associated tracer variability observed with Atmospheric Infrared Sounder
835 (AIRS), J. Geophys. Res., 111, D12314, doi:10.1029/2005JD006490, 2006.

836 Randel, W. J., Moyer, E., Park, M., Jensen, E., Bernath, P., Walker, K., and Boone C.: Global
837 variations of HDO and HDO/H2O ratios in the upper troposphere and lower stratosphere
838 derived from ACE-FTS satellite measurements, J. Geophys. Res., 117, D06303,
839 doi:10.1029/2011JD016632, 2012.

840 Randel, W. J., Park, M., Emmons, L., Kinnison, D., Bernath, P., Walker, K. A., Boone, C. and
841 Pumphrey H.: Asian monsoon transport of pollution to the stratosphere, Science. Apr
842 30,328(5978),611-3. Epub Mar 25, 2010.

843 Rast, S., M.G. Schultz, I. Bey, T. van Noije and co-authors, Evaluation of the tropospheric
844 chemistry general circulation model ECHAM5–MOZ and its application to the analysis
845 of the chemical composition of the troposphere with an emphasis on the late RETRO
846 period 1990–2000 Technical rapport: 2014, Max Planck Institute of Meteorology, Earth
847 System Science, 74p. Real, E., Orlandi, E., Law, K. S., Fierli, F., Josset, D., Cairo, F.,
848 Schlager, H., Borrmann, S., Kunkel, D., Volk, C. M., McQuaid, J. B., Stewart, D. J., Lee,
849 J., Lewis, A. C., Hopkins, J. R., Ravegnani, F., Ulanovski A. and Liousse C.: Cross-
850 hemispheric transport of central African biomass burning pollutants: implications for
851 downwind ozone production, Atmos. Chem. Phys., 10, 3027–3046, 2010.

852 Ridley, B. A., Madronich, S., Chatfield, R. B., Walega, J. G., Shetter, R. E., Carroll, M. A.,
853 and Montzka D. D: Measurements and model simulations of the photostationary state
854 during the Mauna Loa Observatory Photochemistry Experiment: Implications for radical
855 concentrations and ozone production and loss rates, J. Geophys. Res., 97(D10), 10375–
856 10388, doi:10.1029/91JD02287, 1992.
857 Ridley, B.A., J.G. Walega, J.E. Dye, and F.E. Grahek, Distributions of NO, NOx, NOy, and O3
858 to 12 km altitude during the summer monsoon season over New Mexico, *J. Geophys.*
859 *Res., 99*, 25,519-25,534, 1994.
860 Roeckner, E., Bauml, G., Bonaventura, L., Brokopf, R., Esch, M., Giorgetta, M., Hagemann, S.,
861 Kirchner, I., Kornblueh, L., Manzini, E., Rhodin, A., Schlese, U., Schulzweida, U., and
862 Tompkins, A.: The atmospehric general circulation model ECHAM5: Part 1, Tech. Rep.
863 349, Max Planck Institute for Meteorology, Hamburg, 2003.
864 Sander, S. P. Fried, R. R., Barker, J. R., Golden,D. M., Kurylo, M. J. , Wine, P. H., J. Abbatt P.
865 D., Burkholder, J. B., Kolb, C. E., Moortgat, G. K., Huie, R. E., Orkin, V. L.: Chemical
866 kinetics and photochemical data for use in atmospheric studies, evaluation number 14,
867 JPL Publ. 02-25, Jet Propul. Lab., Calif. Inst. of Technol., Pasadena. (Available
868 at http://jpldataeval.jpl.nasa.gov/pdf/JPL_02-25_rev02.pdf), 2003.
869 Schmitz, J. T., Mullen S. L., 1996: Water Vapor Transport Associated with the Summertime
870 North American Monsoon as Depicted by ECMWF Analyses. J. Climate, **9**, 1621–1634.,
871 1996.
872 Schultz, M., Backman, L., Balkanski, Y., Bjoerndalsaeter, S., Brand, R., Burrows, J., Dalsoeren,
873 S., de Vasconcelos, M., Grodtmann, B., Hauglustaine, D., Heil, A., Hoelzemann, J.,
874 Isaksen, I., Kaurola, J., Knorr, W., Ladstaetter-Weienmayer, A., Mota, B., Oom, D.,
875 Pacyna, J., Panasiuk, D., Pereira, J., Pulles, T., Pyle, J., Rast, S., Richter, A., Savage, N.,
876 Schnadt, C., Schulz, M., Spessa, A., Staehelin, J., Sundet, J., Szopa, S., Thonicke, K., van

het Bolscher, M., van Noije, T., van Velthoven, P., Vik, A., and Wittrock, F.: REanalysis of the TROpospheric chemical composition over the past 40 years (RETRO). A long-term global modeling study of tropospheric chemistry. Final Report, Tech. rep., Max Planck Institute for Meteorology, Hamburg, Germany, 2007.

Schultz, M. G., Heil, A., Hoelzemann, J. J., Spessa, A., Thonicke, K., Goldammer, J. G., Held, A. C., Pereira, J. M. C., and van het Bolscher, M.: Global wildland fire emissions from 1960 to 2000, Global Biogeochem. Cy., 22, GB2002, doi:10.1029/2007GB003031, 2008

Schultz, M.G., T. Pulles, R. Brand, M. Van het Bolscher and S.T. Dalsøren, , A global data set of anthropogenic CO, NOx, and NMVOC emissions for 1960-2000, in preparation and available at http://eccad.sedoo.fr/

Schultz, M.G, A. Heil, J.J. Hoelzemann, A. Spessa, K. Thonicke, J. Goldammer, A.C. Held, J.M. Pereira, M. Van Het Bolscher, 2005: Global Wildland Fire Emissions from 1960 to 2000, doi:10.1029/2007GB003031 , Global Biogeochemical Cycles 22 (GB2002) : 17 PP

Schumann, U. and Huntrieser, H.: The global lightning-induced nitrogen oxides source, Atmos. Chem. Phys., 7, 3823–3907, 2007.

Shepon, A., Gildor, H., Labrador, L. J., Butler, T., Ganzeveld, L. N., and Lawrence, M. G.: Global reactive nitrogen deposition from lightning NOx, J. Geophys. Res., 112, D06304, doi:10.1029/2006JD007458, 2007.

Singh, H. B., Viezee, W., Chen, Y., Thakur, A. N., Kondo, Y. and Talbot, R. W.,Gregory, G. L., Sachse, G. W., Blake, D. R., Bradshaw, J. D., Wang, Y., and Jacob D. J.: Latitudinal distribution of reactive nitrogen in the free troposphere over the Pacific Ocean in late

winter/early spring, J. Geophys. Res., 103(D21), 28237–28246, doi:10.1029/98JD01891, 1998.

Singh, H.B., Salas, L.J. and Viezee, W.: Global distribution of peroxyacetyl nitrate, Nature, Jun 5-11;321(6070):588-91, 1986.

Stier, P., Feichter, J., Kinne, S., Kloster, S., Vignati, E., Wilson, J., Ganzeveld, T., Tegen, I., Werner, M., Balkanski, Y., Schulz, M., Boucher, O., Minikin, A., and Petzold, A.: The aerosol climate model ECHAM5-HAM, Atmos. Chem. Phys. 5, 1125– 1165, doi:10.5194/acp-5-1125-2005, 2005.

Talbot, R. W., Dibb, J. E., Scheuer, E. M., Bradshaw, J. D., Sandholm, S. T., Singh, H. B., Blake, D. R., Blake, N. J., Atlas, E., and Flocke, F.: Tropospheric reactive odd nitrogen over the South Pacific in austral springtime, J. Geophys. Res., 105, 6681–6694, doi:10.1029/1999JD901114, 2000.

Talukdar, R. K., Burkholder, J. B., Schmoltner, A., Roberts, J. M., Wilson, R. R. and Ravishankara, A. R.: Investigation of loss processes for peroxyacetyl nitrate in the atmosphere: UV photolysis and reaction with OH, J. Geophys. Res., 100, 14163–14173, 1995.

Tang, J. H., Chan, L. Y., Chang, C. C., Liu, S., and Li, Y. S.: Characteristics and sources of non-methane hydrocarbons in background atmospheres of eastern, southwestern, and southern China, J. Geophys. Res., 114, D03304, doi:10.1029/2008JD010333, 2009.

Tie, X.X., Zhang, R., Brasseur, G., Emmons, L. and Lei, W.: Effects of lightning on reactive nitrogen and nitrogen reservoir species in the troposphere. *Journal of Geophysical Research-Atmospheres*, **106**, 3167-3178, DOI: 10.1029/2000JD900565, 2001.

Vaughan G. and Timmis C.: Transport of near-tropopause air into the lower midlatitude stratosphere, Q. J. R. Meteorol. SOC., 124, pp. 1559-1578, 1998.

Von Clarmann, T., Höpfner, M., Kellmann, S., Linden, A., Chauhan, S., Funke, B., Grabowski, U.,Glatthor, N., Kiefer, M., Schieferdecker, T., Stiller, G. P., and Versick, S.: Retrieval of temperature, H2O, O3, HNO_3, CH_4, N_2O, $ClONO_2$ and ClO from MIPAS reduced

925 resolution nominal mode limb emission measurements, Atmos. Meas. Tech., 2, 159–175,
926 doi:10.5194/amt-2- 2159-2009, 2009.

927 Wiegele A., Glatthor N., Hopfner M., Grabowski U., Kellmann S., Linden A., Stiller G., and von
928 Clarmann T.: Global distributions of C_2H_6, C_2H_2, HCN, and PAN retrieved from MIPAS
929 reduced spectral resolution measurements, Atmos. Meas. Tech., 5, 723–734,
930 doi:10.5194/amt-5-723-2012, 2012,

931 Xiong, X., Houweling, S., Wei, J., Maddy, E., Sun, F., and Barnet, C.: Methane plume over
932 South Asia during the monsoon season: Satellite observation and model simulation,
933 Atmos. Chem. Phys., 9, 783– 794, 2009.

934 Zhang, L, Jacob, D. J., Boersma, K. F., Jaffe, D. A., Olson, J. R., Bowman, K. W., Worden, J.
935 R., Thompson, A. M., Avery, M. A., Cohen, R. C., Dibb, J. E., Flock, F. M., Fuelberg, H.
936 E., L. Huey, G., McMillan, W.W., Singh, H. B., and Weinheimer, A. J.: Transpacific
937 transport of ozone pollution and the effect of recent, Asian emission increases on air
938 quality in North America: an integrated analysis using satellite, aircraft, ozonesonde, and
939 surface observations, Atmos. Chem. Phys., 8, 6117–6136, 2008.

940 Zhao, C., Wang, Y., Choi, Y., and Zeng, T.: Summertime impact of convective transport and
941 lightning NOx production over North America: modeling dependence on meteorological
942 simulations, Atmos. Chem. Phys., 9, 4315–4327, 2009.

943 Ziereis, H., H. Schlager, P. Schulte, P.F.J. van Velthoven, and F. Slemr, Distributions of NO,
944 NOx, and NOy in the upper troposphere and lower stratosphere between 28°N and 61°N
945 during POLINAT 2, *J. Geophys. Res.*, **105**, 3653, 2000.

946

947

948 Table 1: Global aircraft measurements used for model evaluation.

Experiment	Date Frame	Species	Location
POLINAT-2 (Falcon) Ziereis et al.2000	Sep 19-Oct 25, 1997	O3, NOX	Canary-Islands:LAT= 25., 35. LON=340., 350. E-Atlantic:LAT= 35., 45.LON=330.,340. Europe: LAT= 45.,55. LON=5.,15. Ireland: LAT=50., 60. LON= 345.,355.
PEM-Tropics-A (DC8) Talbot et al. (2000)	Aug 24-Oct 15, 1996	O3, NOX, HNO3, PAN	Christmas-Island: LAT= 0., 10. LON=200., 220. Easter-Island: LAT=-40.,-20.LON=240., 260. Fiji: LAT= -30.,-10. LON= 170., 190. lawaii: LAT= 10., 30. LON= 190., 210. Tahiti: LAT= -20., 0. LON= 200., 230.
PEM-Tropics-A (P3) O'Sullivan et al, 1999	Aug 15-Sep 26, 1996	O3, HNO3	Christmas-Island: LAT= 0., 10. LON= 200., 220. Easter-Island: LAT= -40.,-20. LON= 240., 260. Hawaii: LAT= 10., 30. LON= 190., 210. Tahiti: LAT= -20., 0. LON= 200., 230.
ABLE-3B (Electra) Harriss et al.,1994	Jul 6-Aug 15, 1990	O3, NOX, HNO3, PAN	Labrador: LAT= 50., 55. LON= 300., 315. Ontario: LAT= 45., 60. LON= 270., 280. US-E-Coast: LAT= 35., 45. LON= 280., 290.
CITE-3 (Electra) Hoell et al 1993	Aug 22-Sep 29, 1989	O3, NOX	Natal: LAT= -15.,5. LON= 325., 335. Wallops: LAT= 30., 40. LON= 280., 290.
ELCHEM (Sabreliner) Ridley et al.,1999	Jul 27-Aug 22, 1989	O3, NOX	New-Mexico: LAT=30., 35. LON= 250., 255.
ABLE-3A (Electra) Harriss et al.,1992	Jul 7-Aug 17, 1988	O3, NOX ,PAN	Alaska: LAT= 55., 75. LON= 190., 205.
ABLE-2A (Electra) Harris et al., 1988	Jul 12-Aug 13, 1985	O3	E-Brazil: LAT= -10., 0. LON= 300., 315. W-Brazil: LAT= -5., 0. LON= 290., 300.
STRATOZ-3 (Caravelle 116) Drummond et al., 1988	Jun 4-26, 1984	O3	Brazil: LAT= -20.,0. LON= 315., 335. Canary-Islands: LAT= 20.,35. LON= 340., 355. E-Tropical-N-Atlantic: LAT= 0.,20.LON=330.,345. England: LAT= 45., 60. LON= -10., 5. Goose-Bay: LAT= 45., 60. LON= 290., 305. Greenland: LAT= 60., 70. LON= 290., 330. Iceland: LAT= 60., 70. LON= 330., 355. NW-South-America: LAT=-5., 10. LON= 275.,295. Puerto-Rico: LAT= 10., 25. LON= 290., 300. S-South-America: LAT= -65.,-45. LON= 275., 300. SE-South-America: LAT= -45.,-20. LON= 295.,320. SW-South-America: LAT=-45.,-25. LON= 285.,292. Spain: LAT= 35., 45. LON= -15., 0. W-Africa: LAT= 0., 15. LON= -15., 0. W-South-America: LAT= -25., -5. LON= 275.,290. Western-N-Atlantic: LAT= 25., 45.LON= 290.,300.
CITE-2 (Electra) Hoell et al., 1990	Aug 11-Sep 5, 1986	O3, NO_X, HNO_3, PAN	Calif: LAT= 35., 45. LON= 235., 250. Pacific: LAT= 30., 45. LON= 225., 235.
CAIPEEX Prabha et al., 2011)	Sep 2010 –Oct 2010	O_3, NO_X	Lat=17^0N, Lon=78^0E

949

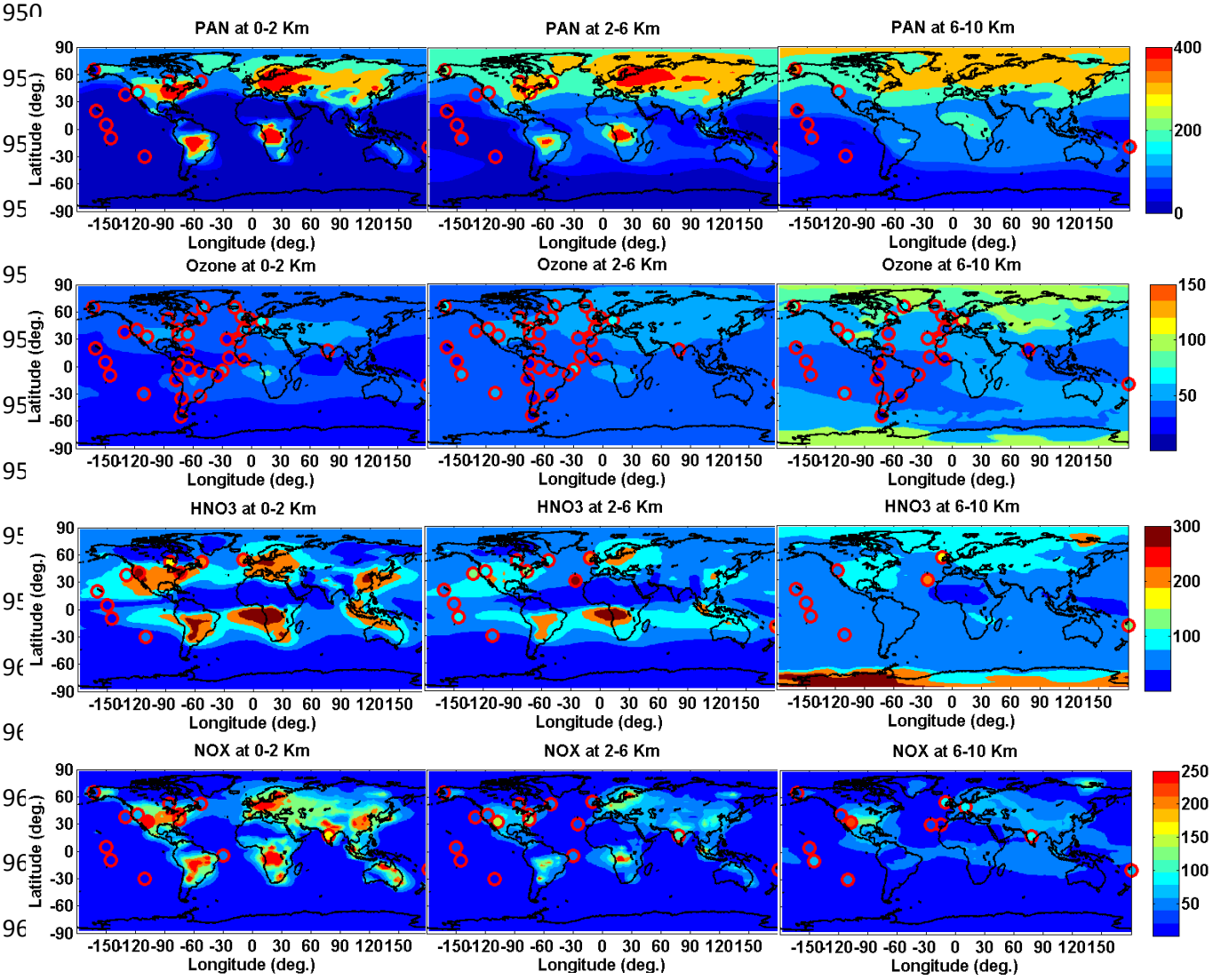

Figure 1 Global mean distribution of PAN (ppt), ozone (ppb), HNO_3 (ppt), NO_X (ppt) for monsoon seasons and altitude ranges. Model results for 1995-2004 (background solid contours) are compared to aircraft observations from Table 1 for all years (filled circles). Aircraft observations are averaged vertically and horizontally over the coherent regions.

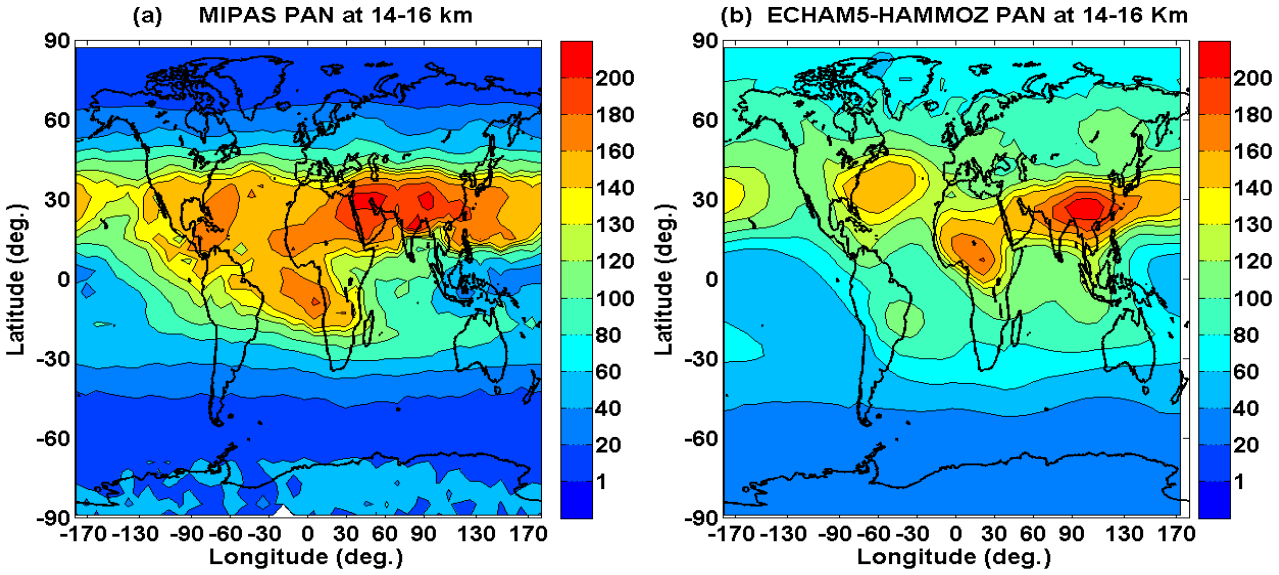

Figure 2. Distribution of seasonal mean PAN concentration (ppt) as observed by MIPAS-E (climatology for the period 2002-2011) at (a) 14 km (b) 16 km and ECHAM5-HAMMOZ CTRL simulations at (c) 14km (d) 16km. ECHAM5-HAMMOZ simulations are smoothed with averaging kernel of MIPAS-E.

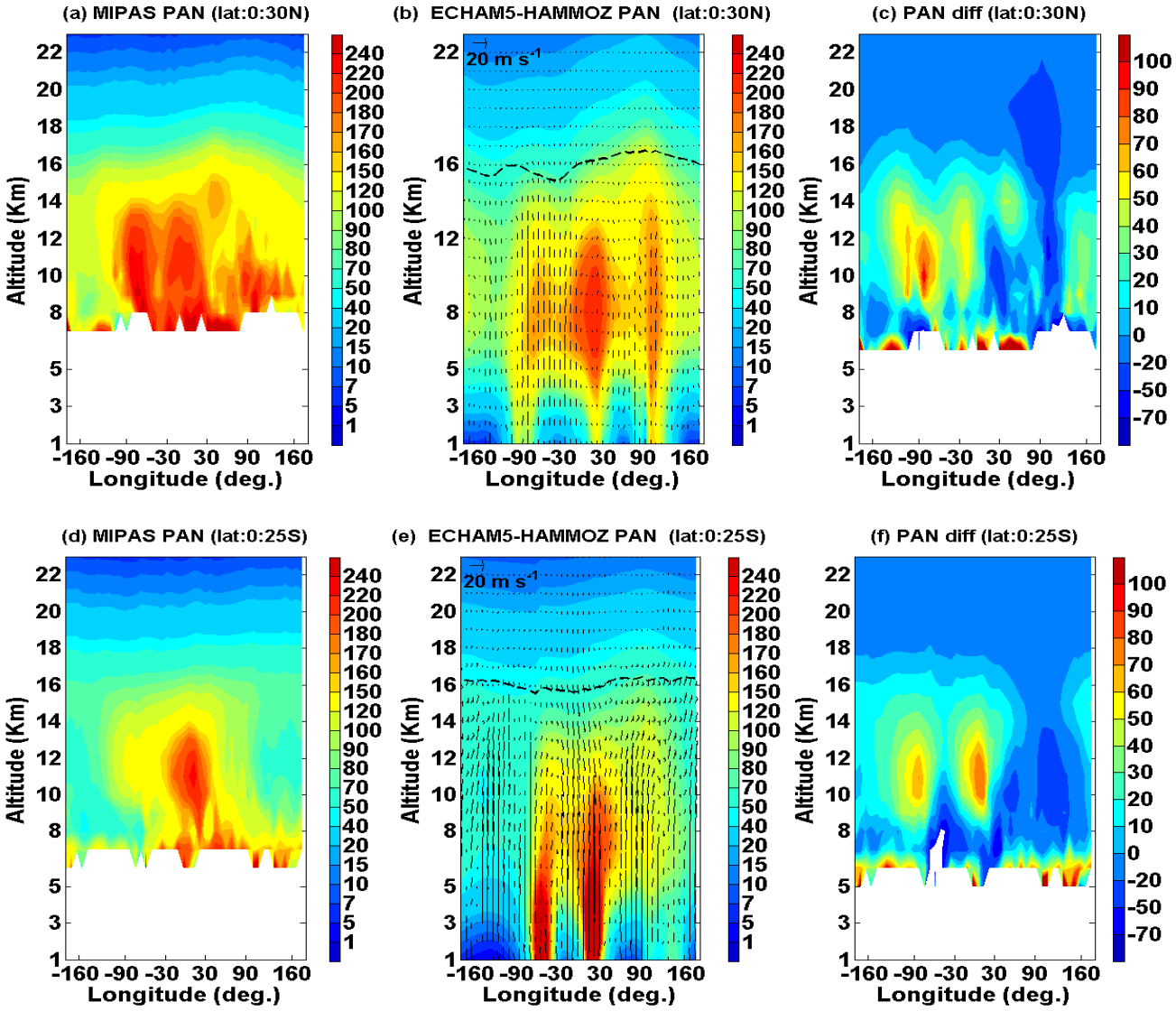

Figure 3. Longitude-altitude cross section of PAN (ppt) averaged for monsoon season and 10N-30^{O}N (a) MIPAS-E climatology (b) ECHAM5-HAMMOZ CTRL simulations. (c) difference in PAN (ppt) (MIPAS-ECHAM5-HAMMOZ).PAN (ppt) averaged for monsoon season and 0-25^{O}S (d) MIPAS-E climatology (e) ECHAM5-HAMMOZ CTRL simulations (f) difference in PAN (ppt) (MIPAS-ECHAM5-HAMMOZ). ECHAM5-HAMMOZ simulations are smoothed with averaging kernel of MIPAS-E. Wind vectors are indicated by black arrows in figures (b) and (e). The vertical velocity field has been scaled by 300. We consider MIPAS data between 8 km and 23km.

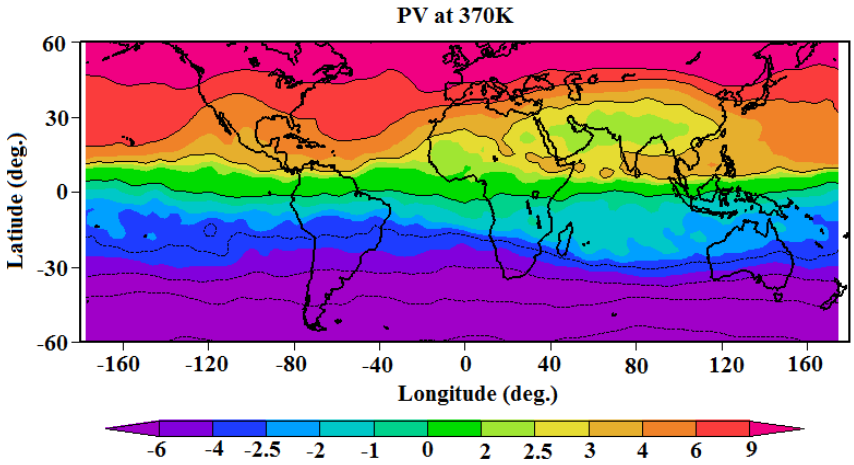

Figure 4. The map of PV in PV units (1 PVU = 10^{-6} K m^2 kg^{-1} s^{-1}) on the 370 K level for the monsoon season obtained from ECHAM5-HAMMOZ CRTL simulations.

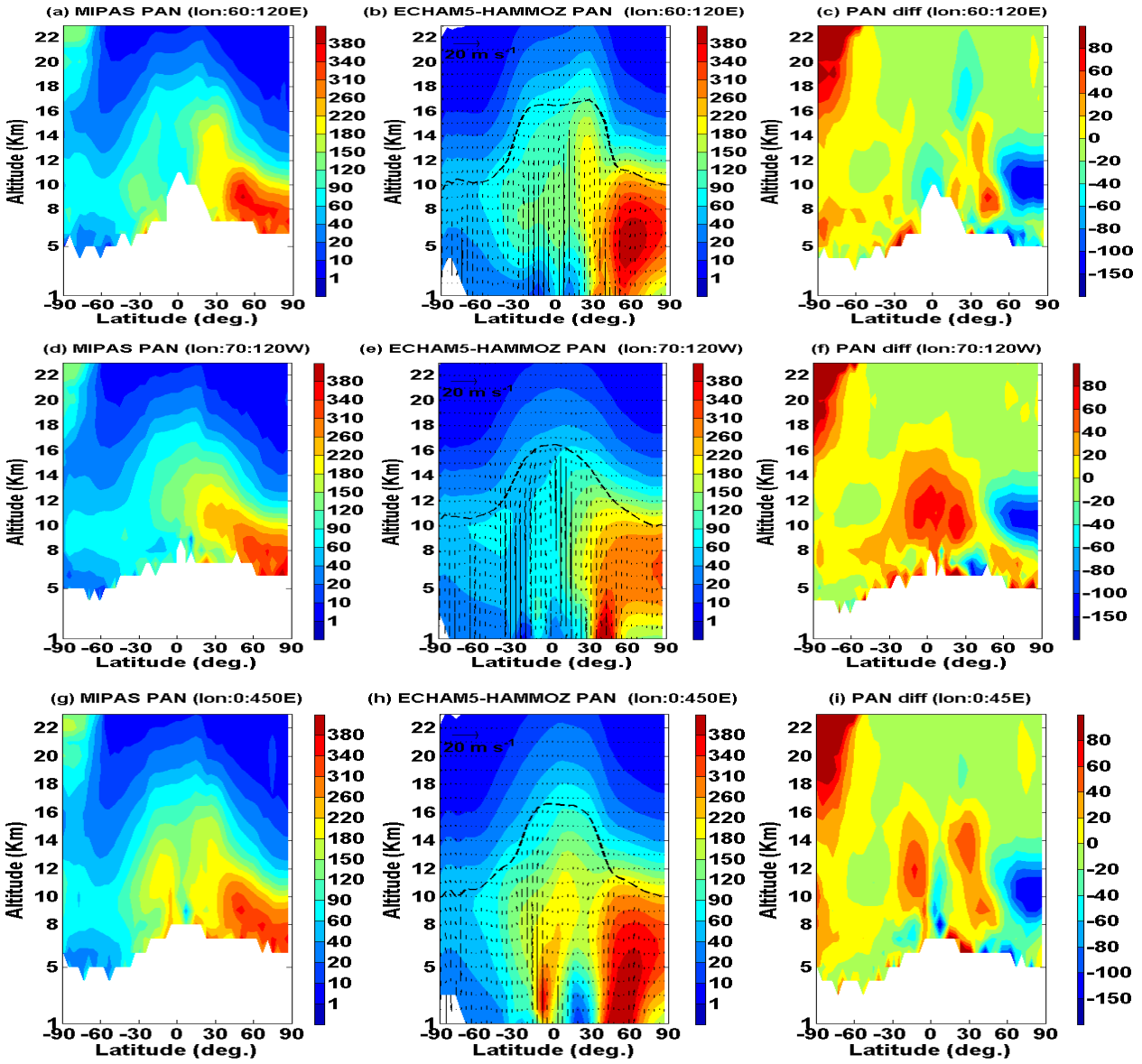

Figure 5. Latitude-altitude cross section of PAN (ppt) (a) MIPAS-E climatology, averaged for monsoon season and 60-120^{O}E, (b) PAN from ECHAM5-HAMMOZ CTRL simulations, , averaged for monsoon season and 60-120^{O}E, (c) difference in PAN (ppt) (MIPAS-ECHAM5-HAMMOZ). (d) same as (a) but averaged over 70W-120^{O}W (e) same as (b) but averaged over 70W-120^{O}W (f) difference in PAN (ppt) (MIPAS-ECHAM5-HAMMOZ). (g) same as (a) but averaged over 0-45^{O}E (h) same as (b) but averaged for 0-45^{O}E (i) difference in PAN (ppt) (MIPAS-ECHAM5-HAMMOZ).. Wind vectors are indicated by black arrows in figures (b), (e)

and (f). The vertical velocity field has been scaled by 300. . We consider MIPAS data between 8 km and 23km.

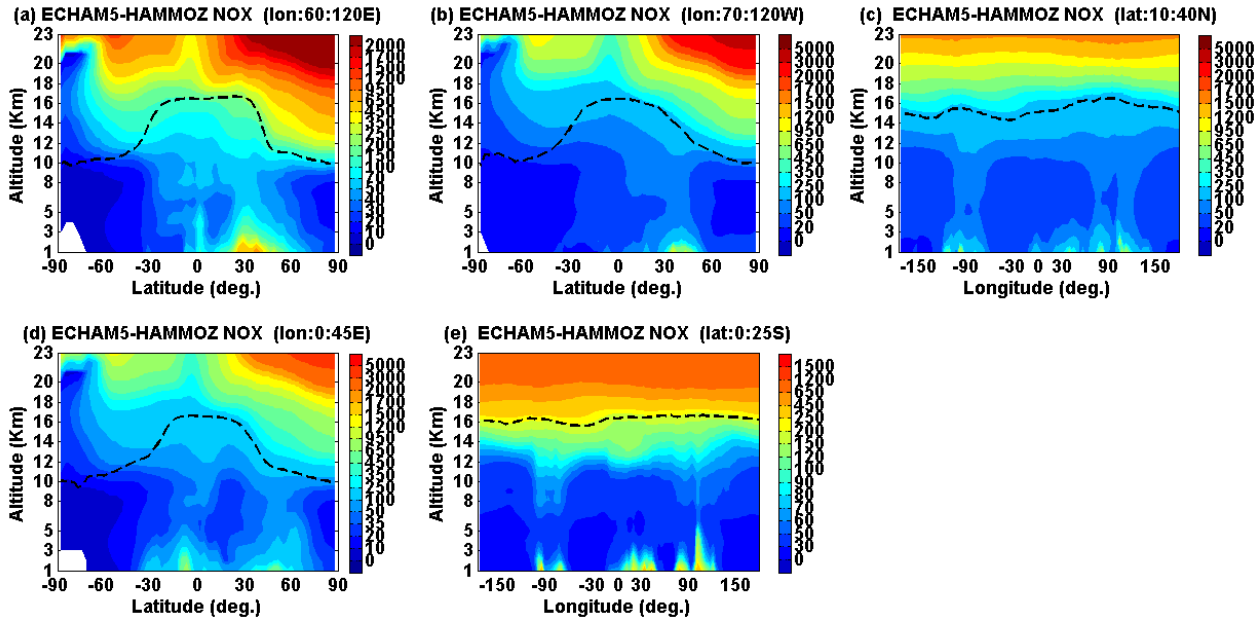

Figure 6. Panel (a) Latitude-altitude cross section of seasonal mean ECHAM5-HAMMOZ NO_X (ppt) averaged for (a) 60-120^{O}E (b) 70W-120^{O}W (c) 10-40^{O}N (d) 0-45^{O}E and (e) 0-25^{O}S.

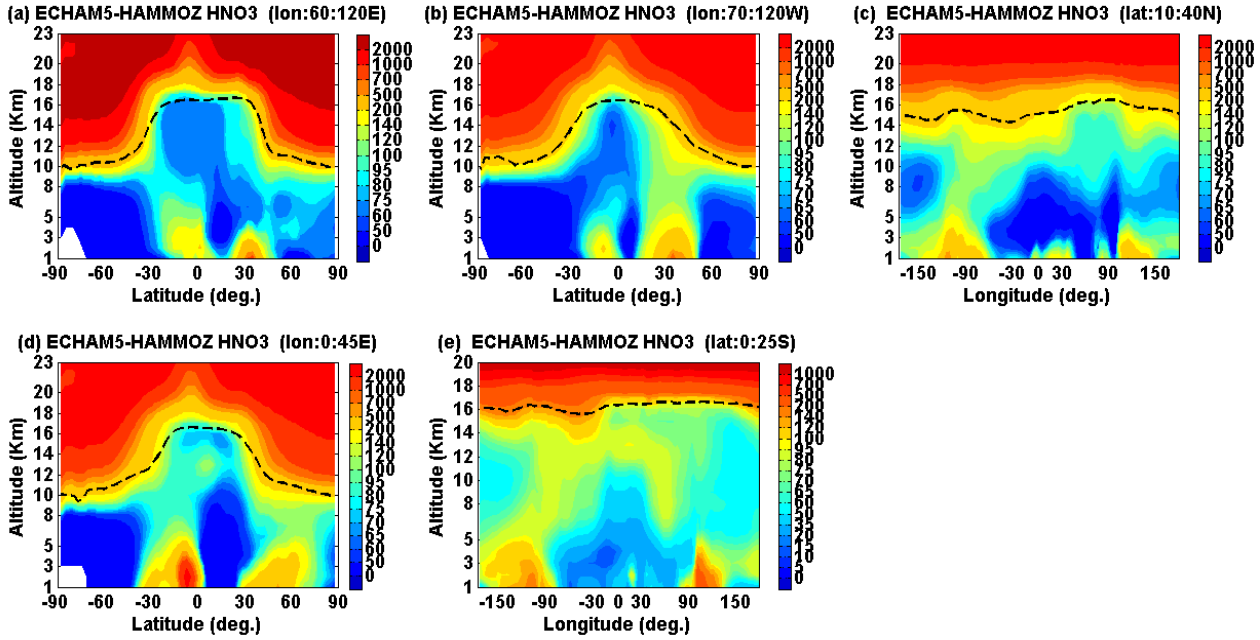

Figure 7. same as figure6 but for HNO_3 (ppt).

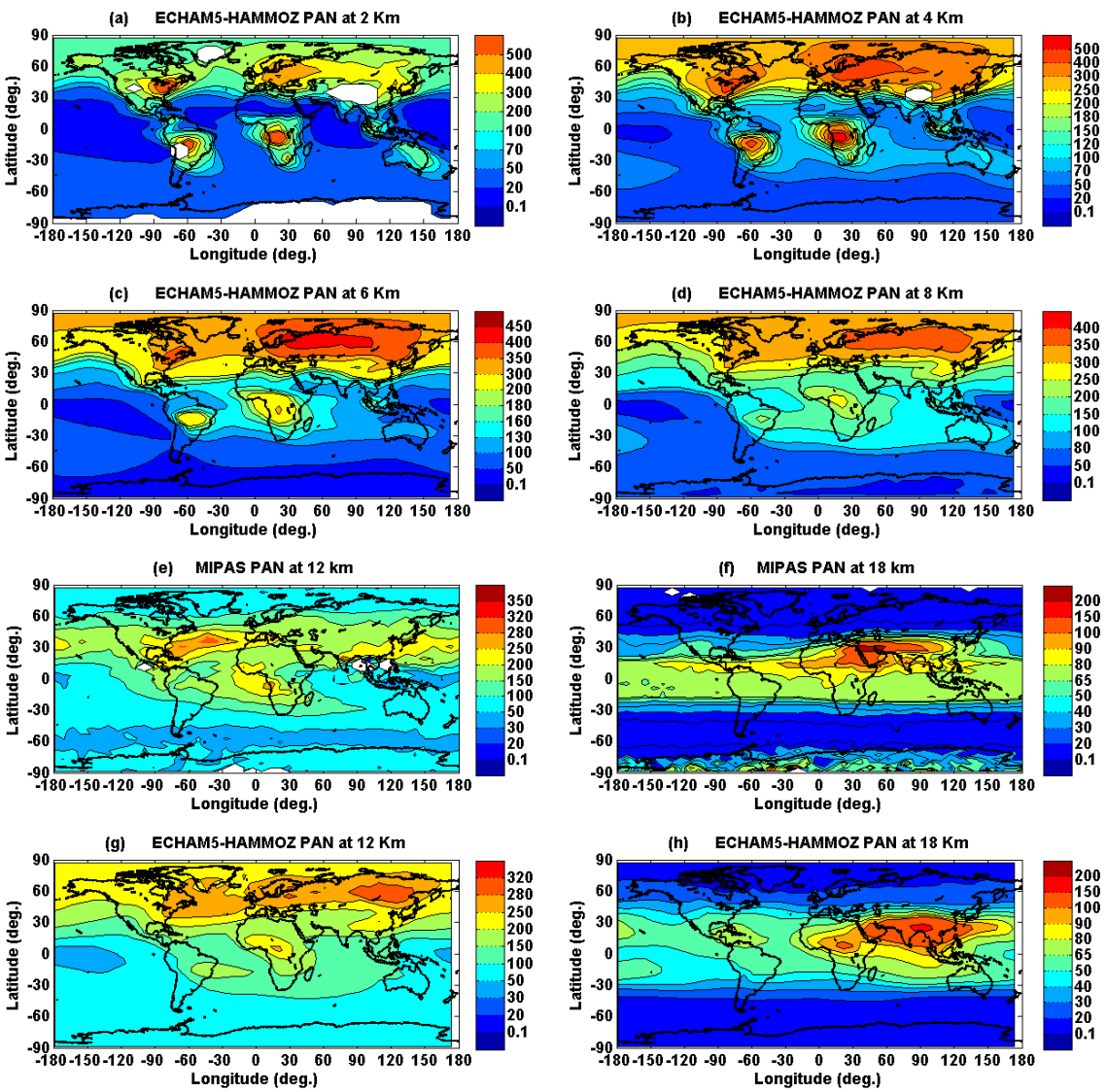

Figure 8. Latitude-longitude cross section of PAN (ppt) averaged for monsoon season (a) ECHAM5-HAAMOZ simulations at 1km (b) 3km (c) 6km (d) 8km. MIPAS-E climatology at (e) 12km (f) 18 km. ECHAM5-HAMMOZ CTRL simulation at (g) 12 km (h) 18km.

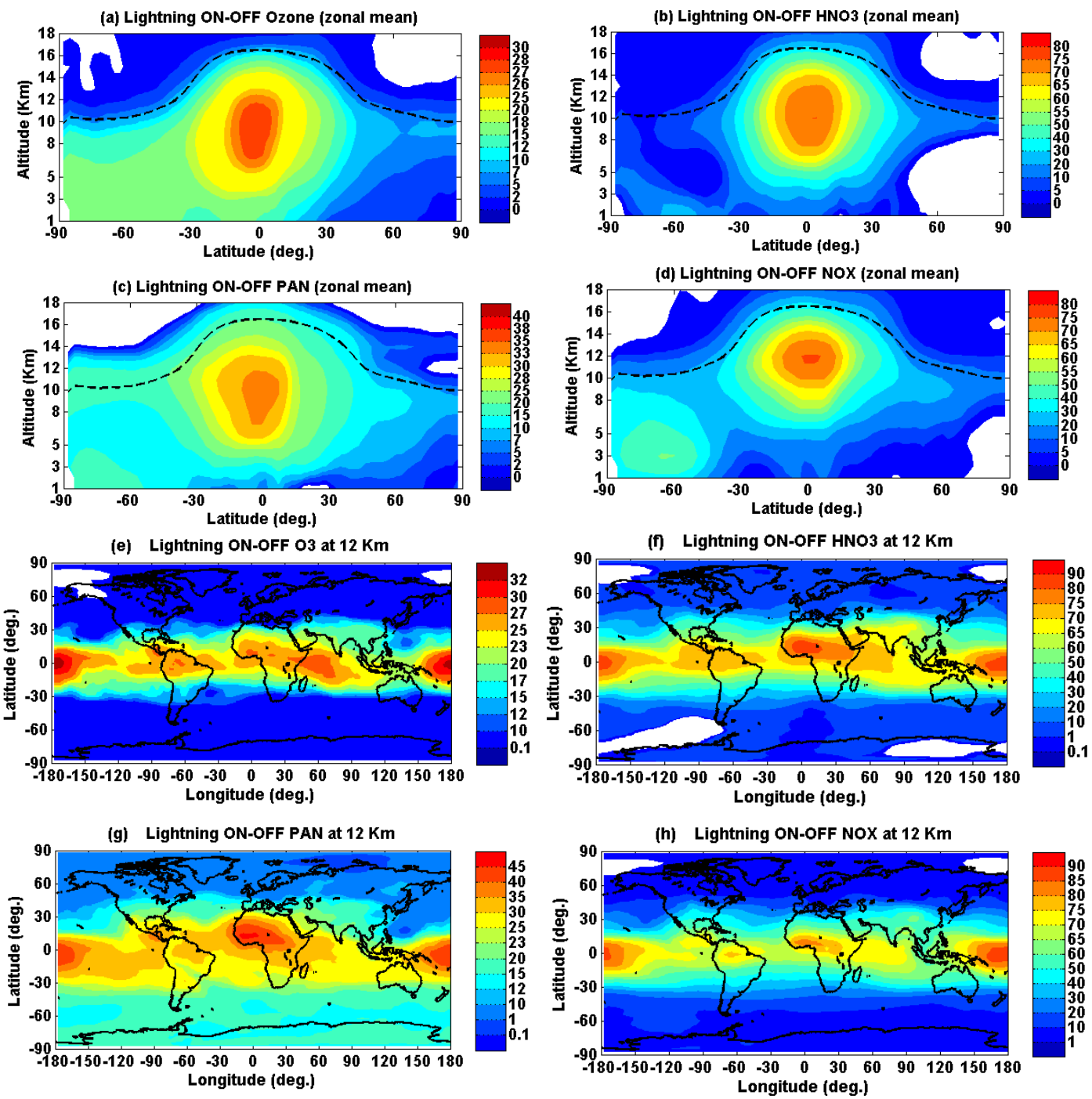

Figure 9: Zonally averaged seasonal mean changes (percentage) produced from lightning in (a) ozone (b) HNO_3 (c) PAN (d) NO_X, distribution of seasonal mean changes (percentage) produced from lightning in (e) ozone (f) HNO_3 (g) PAN (h) NO_X at 12km.

Supplementary figures

(a) **(b)**

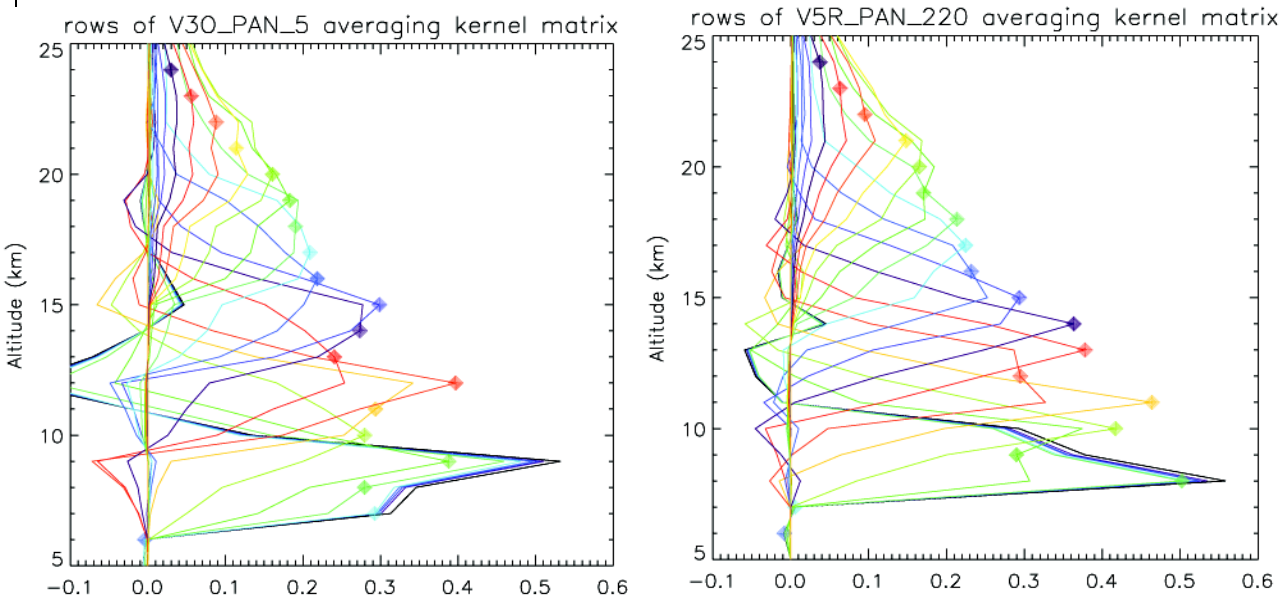

Figure S1: The averaging kernel rows of (a) V3O_PAN_5 at the location 26^{O} N and 81^{O} E and (b) V5R_PAN_220 at the location 28 ^{O} N and 85 ^{O} E. Diamonds indicate the respective nominal altitudes of the retrieval grid.

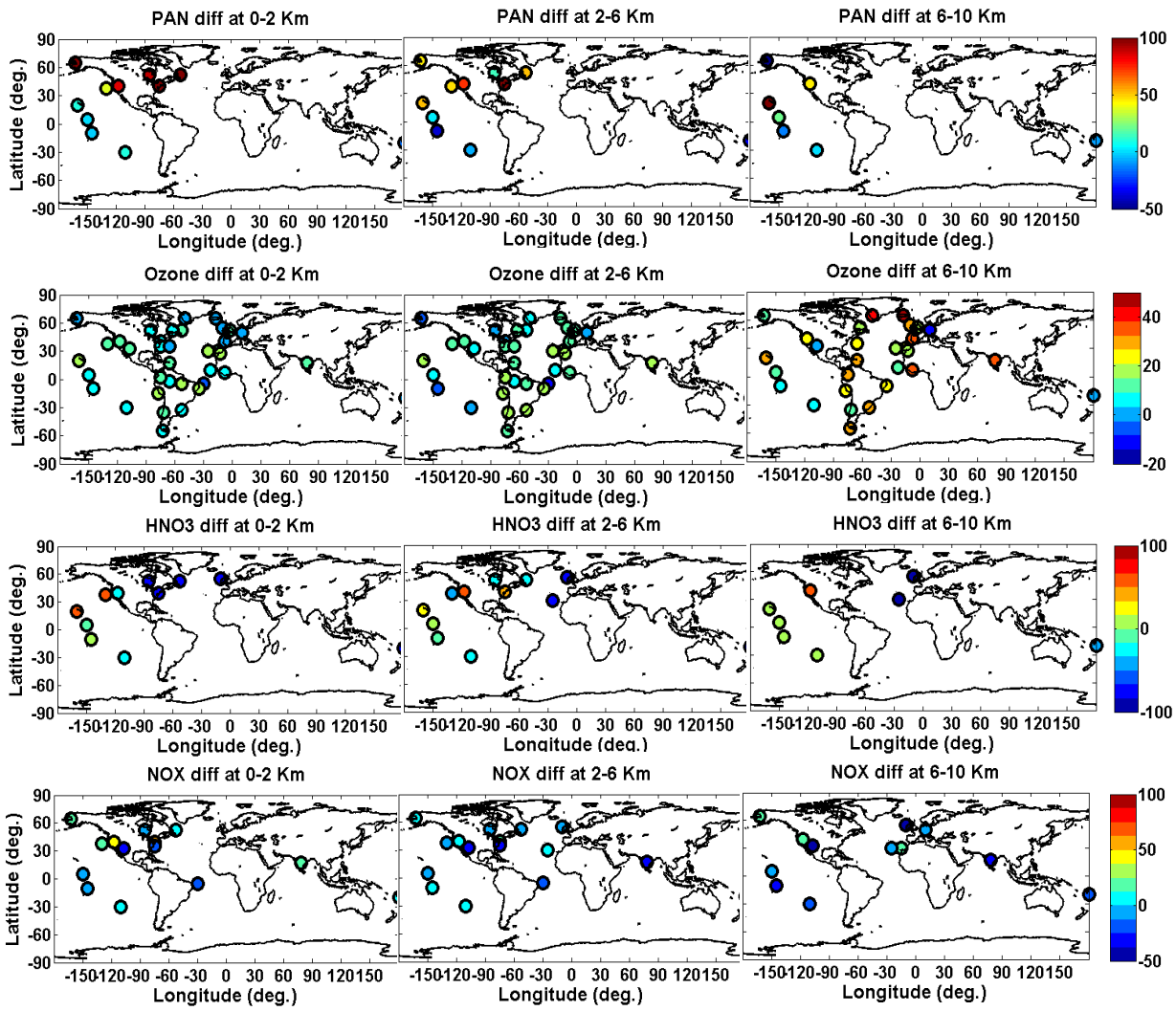

Figure S2: Global distribution of bias (ECHAM5-HAMMOZ – aircraft observations) in PAN (ppt), ozone (ppb), HNO_3 (ppt), NO_X (ppt) for monsoon season and altitude ranges.

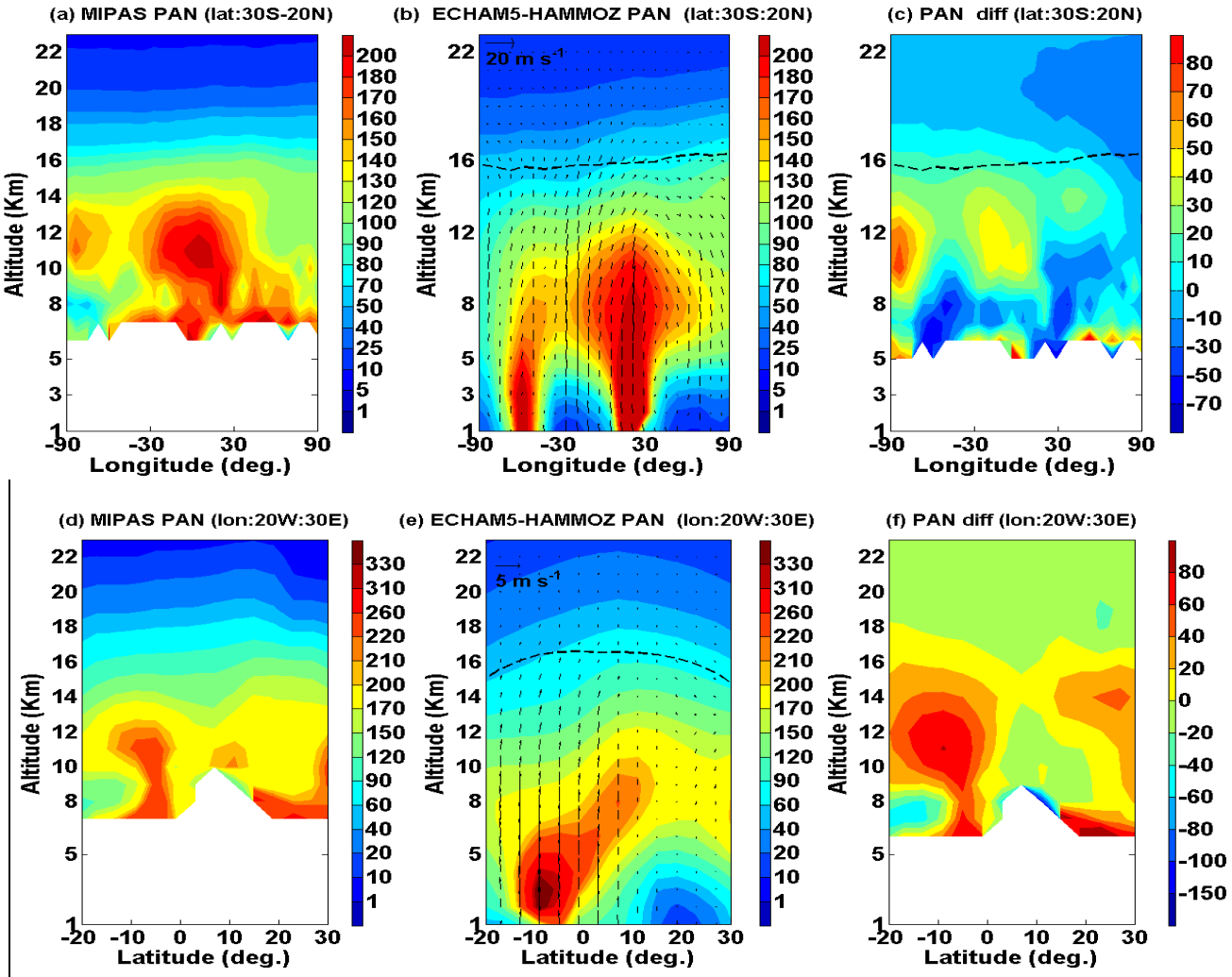

Figure S3 : Longitude –altitude cross-section of PAN (ppt) averaged for monsoon season and over 30S-20N (a) MIPAS-E climatology (b) ECHAM5-HAMMOZ CTRL simulations (c) difference in PAN (ppt) (MIPAS-ECHAM5-HAMMOZ). Latitude-altitude cross-section of PAN (ppt) averaged for monsoon season and over 20W-30E (d) MIPAS-E climatology (e) ECHAM5-HAMMOZ CTRL simulations (f) difference in PAN (ppt) (MIPAS-ECHAM5-HAMMOZ). We consider MIPAS data between 8 km and 23km.

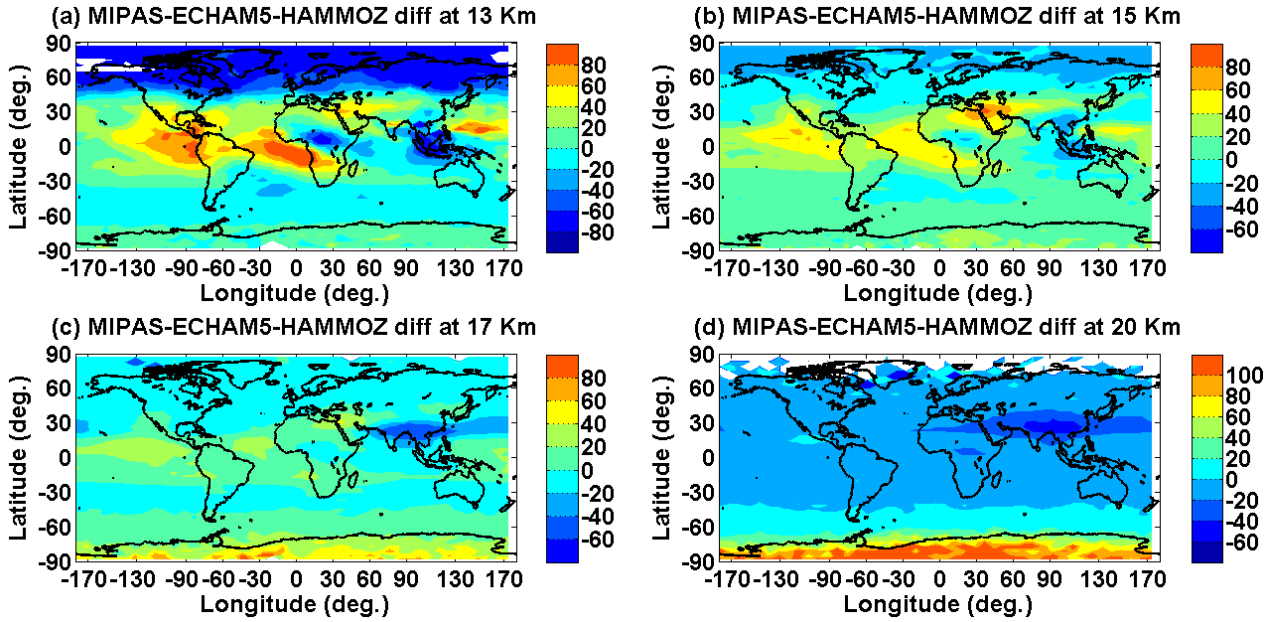

Figure S4: Differences between MIAPS observations (climatology 2002-2011) and ECHAM5-HAMMOZ reference simulation in PAN (ppt) averaged for the monsoon season (a) at 13km (b) 15km (c) 17 km and (d)19km.

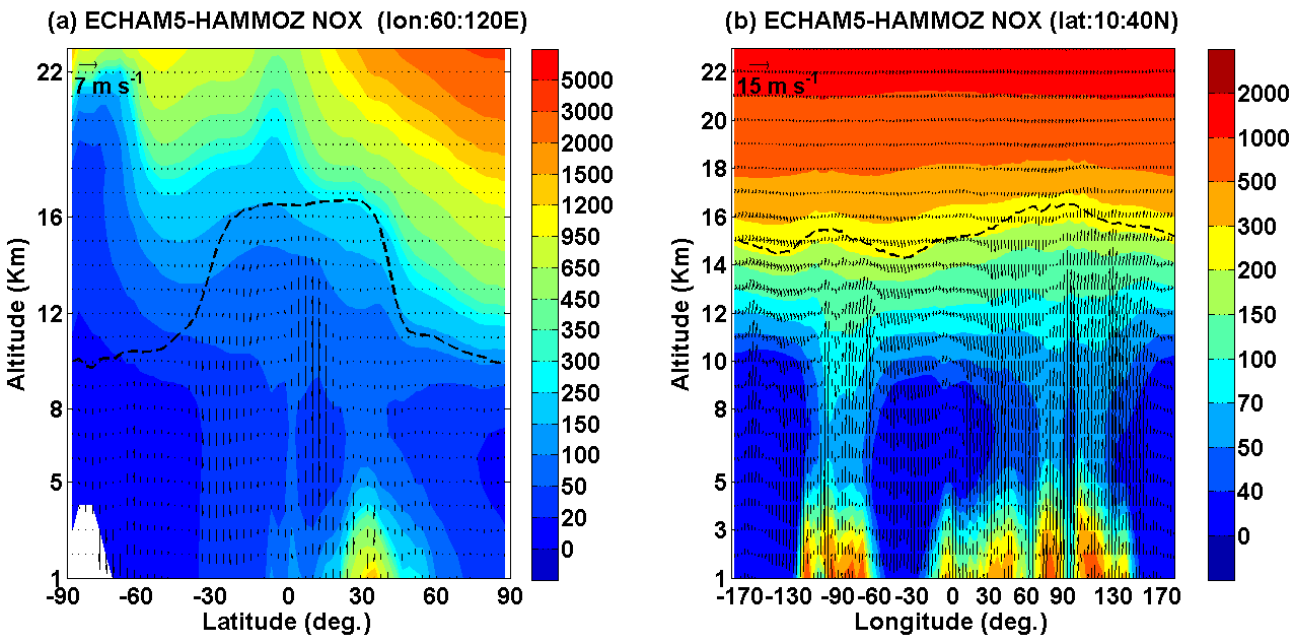

Figure S5. Latitude-pressure cross section of seasonal mean ECHAM5-HAMMOZ NOX (ppt) obtained from reference simulation (a) averaged for 60-120E (b) averaged for 12-40N. The black arrows indicate wind vectors. The vertical velocity field has been scaled by 300.